AperTO - Archivio Istituzionale Open Access dell'Università di Torino

Very hot, very shallow hydrothermal dolomitization: An example from the Maritime Alps (north-west Italy–south-east France)

This is the author's manuscript

Original Citation:

Availability:

This version is available http://hdl.handle.net/2318/1618351 since 2018-06-15T12:33:56Z

Published version:

DOI:doi: 10.1111/sed.12294

Terms of use:

Open Access

Anyone can freely access the full text of works made available as "Open Access". Works made available under a Creative Commons license can be used according to the terms and conditions of said license. Use of all other works requires consent of the right holder (author or publisher) if not exempted from copyright protection by the applicable law.

(Article begins on next page)

18 August 2024

UNIVERSITÀ DEGLI STUDI DI TORINO

This is the author's final version of the contribution published as:

Luca Barale, Carlo Bertok, Namam Salih Talabani, Anna d'Atri, Luca Martire, Fabrizio Piana, Alain Préat. Very hot, very shallow hydrothermal dolomitization: An example from the Maritime Alps (north-west Italy–south-east France). SEDIMENTOLOGY. None pp: 1-29.

DOI: doi: 10.1111/sed.12294

When citing, please refer to the published version.

Link to this full text:
http://hdl.handle.net/

This full text was downloaded from iris - AperTO: https://iris.unito.it/

iris - AperTO

University of Turin’s Institutional Research Information System and Open Access Institutional Repository

VERY HOT, VERY SHALLOW HYDROTHERMAL DOLOMITIZATION: AN EXAMPLE FROM THE MARITIME ALPS (NW ITALY – SE FRANCE)

Luca Barale[1*], Carlo Bertok[1], Namam Salih Talabani[2,3], Anna d'Atri[1], Luca Martire[1], Fabrizio Piana[4], Alain Préat[2]

1: Dipartimento di Scienze della Terra, Università di Torino, Via Valperga Caluso 35, 10125 Torino.

2: Department of Earth and Environmental Sciences, Université Libre de Bruxelles, 50, avenue F. D. Roosevelt, CP 160/02. B-1050 Brussels. Belgium.

3: Petroleum Geosciences Department, Soran University, Delizian, Soran/Erbil, Iraq-Kurdistan.

4: CNR IGG – Torino, Via Valperga Caluso 35, 10125 Torino.

* Corresponding author. E-mail: luca.barale@hotmail.it

Running head: Very hot, very shallow hydrothermal dolomitization

ABSTRACT

In the Maritime Alps (NW Italy–SE France), the Middle Triassic–lowermost Cretaceous platform carbonates of the Provençal Domain locally show an intense dolomitization. Dolomitized bodies, irregularly shaped and variable in size from some metres to hundreds of metres, are associated with tabular bodies of dolomite-cemented breccias, cutting the bedding at a high angle, and networks of dolomite veins. Field and petrographic observations indicate that dolomitization was a polyphase process, in which episodes of hydrofracturing and host-rock dissolution, related to episodic expulsion of overpressured fluids through faults and fracture systems, were associated with phases of host-rock dolomitization and void cementation. Fluid inclusion analysis indicates that dolomitizing fluids were relatively hot (170–260 °C). The case study represents an outstanding example of a fossil hydrothermal system, which significantly contributes to the knowledge of such dolomitization systems in continental margin settings. The unusually favourable stratigraphic framework allows precise constraint of the timing of dolomitization (earliest Cretaceous), and, consequently, direct evaluation of the burial setting of dolomitization, which, for the upper part of the dolomitized succession, was very shallow or even close to the surface. The described large-scale hydrothermal system was probably related to deep-rooted

faults, and provides indirect evidence of a significant earliest Cretaceous fault activity in this part of the Alpine Tethys European palaeomargin.

Keywords: hydrothermal dolomitization, fault-related fluid circulation, Early Cretaceous, Provençal Domain, Maritime Alps

INTRODUCTION

In the broad field of dolomite literature, hydrothermal dolomitization processes (sensu Machel and Lonnee, 2002; Machel, 2004; Davies and Smith, 2006) represent the most studied and discussed in recent years. In fact, beyond the scientific significance, hydrothermal dolostones also have a high economic value, as they have long been known to host important base metal mineralizations (e.g. Mississippi Valley-Type lead–zinc ores; Hewett, 1928). More recently they have been recognized as potentially good hydrocarbon reservoirs (Davies and Smith, 2006, and references therein). Moreover, the upflow of high-temperature fluids through a column of sediments can force the maturation of the organic matter and influence the migration of hydrocarbons (e.g. Lavoie *et al*., 2005; Sharp *et al*., 2010; Guo *et al*., 2011).

In recent years, many examples of hydrothermal dolomitization have been documented worldwide (e.g. Boni *et al*., 2000; Lapponi *et al*., 2007, 2014; López-Horgue *et al*., 2010; Nader *et al*., 2012; Swennen *et al*., 2012; Haeri-Ardakani *et al*., 2013a, b; Hendry *et al*., 2015). In the Alpine chain, several examples of hydrothermal dolomitization come from the Southern Alps (Spencer-Cervato and Mullis, 1992; Carmichael and Ferry, 2008; Carmichael *et al*., 2008; Ferry *et al*., 2011; Ronchi *et al*., 2011, 2012). In many of these study cases, the most challenging point is the timing and the burial depth of dolomitization, which can be only inferred on the basis of indirect evidence regarding the regional context and the burial history.

In the Maritime Alps (NW Italy–SE France), the Middle Triassic and the Middle Jurassic–Berriasian carbonates of the Provençal Domain are locally affected by intense dolomitization in an area of some tens of square kilometres, between the Vermenagna, Gesso, and Sabbione valleys to the north and the Roya and Bieugne valleys to the south (Fig. 1, 2). The presence of these dolostones has already been reported, although very briefly, by Bigot *et al*. (1967), Campanino Sturani (1967), Carraro *et al*. (1970), and Malaroda (1970, 1999). A preliminary description of this phenomenon has been given by Barale *et al*. (2013a), who documented its hydrothermal character, whereas Barale *et al*. (2016) mapped the distribution of dolomitization in the Italian part of the study area. The aim of this paper is to provide the full dataset of field, petrographic, and geochemical characteristics of this remarkable study case of hydrothermal dolomites. The broad significance of this study case derives from the following points:

- local stratigraphy strictly constrains the timing and the burial depth of the dolomitization: the latter is considerably shallower than those reported in previous literature cases;

- inferred temperatures of dolomitizing fluids are very high, considering the shallow subsurface dolomitization environment; and

- it is the first report of hydrothermal dolomite in the Western Alps, where it contributes to a better knowledge of an Early Cretaceous syndepositional tectonics.

GEOLOGICAL SETTING

The Mesozoic succession of the study area was deposited on the European palaeomargin of the Alpine Tethys, in the northern part of the Provençal platform, close to the transition to the Dauphinois basin (Carraro *et al*., 1970; Lanteaume 1990; Barale *et al*., 2016; d'Atri et al., 2016). The Provençal succession starts with Permian continental sediments resting on the crystalline basement of the Argentera Massif, characterized by marked changes in thickness and reaching a maximum thickness of 3000–4000 metres (Faure-Muret, 1955). They are followed by some tens of metres of Lower Triassic coastal siliciclastic deposits, Middle Triassic peritidal carbonates, a few hundred metres thick, and Upper Triassic evaporites. Discrete stratigraphic intervals of Middle Triassic carbonates consist of finely crystalline dolostones that are widespread at the regional scale (e.g., Lanteaume, 1968; Carraro et al., 1970; Costamagna, 2013). A regional discontinuity surface corresponding to a Late Triassic–Early Jurassic hiatus is followed by 200–300 m of platform limestones attributed to the Middle Jurassic–Berriasian (Garbella Limestone; Barale, 2014; Barale *et al*., 2016). Lower Cretaceous deposits are represented by a condensed succession of bioclastic limestones and marly limestones, locally rich in authigenic minerals (phosphates, glauconite), reaching a maximum thickness of some tens of metres (Lanteaume, 1968; Malaroda, 1999; Barale *et al*., 2013b). They are followed by hemipelagic deposits of Late Cretaceous age. In the northern part of the study area (roughly corresponding to the Italian part), Cretaceous deposits are in general thinner and locally absent (Carraro *et al*., 1970; Barale *et al*., 2016). To the northwest of the study area, the Provençal successions pass to thicker Dauphinois successions, characterized by several hundred metres of pelagic to hemipelagic Jurassic–Cretaceous deposits (Carraro *et al*., 1970; Barale *et al*., 2016). The transition between the Provençal platform and Dauphinois basin corresponds to a preserved primary feature (Caire Porcera palaeomargin), which originated as a fault-related palaeo-escarpment during the Early–Middle Jurassic and was subsequently covered by Cretaceous slope deposits (Barale, 2014; Barale *et al*., 2016; d'Atri *et al*., 2016). The top of the Mesozoic succession is truncated by a regional unconformity, corresponding to a hiatus spanning the latest Cretaceous–middle Eocene, overlain by the Alpine Foreland Basin succession. This consists of middle Eocene Nummulitic Limestone (mixed carbonate–siliciclastic ramp deposits), followed by the hemipelagic upper Eocene *Globigerina* Marl and by the upper Eocene–lower Oligocene turbidite succession of the Grès d'Annot (Sinclair, 1997). Since the Eocene, the palaeo-European continental margin has been progressively involved in the ongoing formation of the Alpine belt (e.g., Dumont *et al*., 2012). All the study successions underwent at least three deformation events that were well recorded at a regional scale, firstly with outward (southwestward) brittle–ductile thrusting and superposed foldings, then northeastward back-vergent folding, and lastly southward brittle thrusting and flexural folding (d'Atri *et al*., 2016). The regional structural setting resulted from a transpressional regime with important strain partitioning of contractional versus strike-slip-related structural associations (Piana *et al*., 2009; d'Atri *et al*., 2016), as evidenced by the occurrence of a post-Oligocene NW–SE Alpine transcurrent shear zone (Limone Viozene Zone) extending for several kilometres from Tanaro valley to the study area. This shear zone is probably superimposed on a long-lived shearing corridor active since the Jurassic–Cretaceous and reactivated during the Cenozoic (Bertok et al., 2012; d'Atri et al., 2016). Stratigraphic and geometric evidence of Cretaceous paleofaults have been locally described in nearby sectors (e.g. Bertok et al., 2012), but commonly, in the study area, the large amount of finite deformation related to Alpine tectonics hinders direct recognition of ancient structures.Hydrothermal dolomitization affects the whole Provençal succession from the Middle Triassic carbonates to the Middle Jurassic–Berriasian shallow-water Garbella Limestone (Fig. 3). The Middle Triassic carbonates are represented by a 150–200-m-thick succession of limestones, dolomitic limestones, and fine-grained dolostones, with decimetre-thick bedding (Bersezio and d'Atri, 1986; Malaroda, 1999). Common sedimentary structures are microbial/algal lamination, collapse breccias, flat pebble breccias, tepees, and millimetre-sized calcite pseudomorphs on gypsum crystals, all reflective of a peritidal depositional environment. An interval of dark-coloured, organic-rich limestones and dolostones, a few tens of metres thick, is locally present above the Middle Triassic carbonates (Mont Chajol, see Fig. 2) and is attributed to the Upper Triassic (Malaroda, 1999).

The Garbella Limestone is a 200–300-m-thick platform succession organized in poorly-defined decimetre- to metre-thick beds and mainly consisting of bioclastic packstones to rudstones and boundstones, rich in echinoderm fragments, corals, nerineid gastropods (e.g. *Ptygmatis pseudobruntrutana*), rudists (Diceratidae), and stromatoporoids. In the upper part, bioclastic mudstones–wackestones with *Clypeina jurassica* are common. The uppermost 5–10 metres are locally represented by peritidal limestones associated with lagoonal charophyte-rich wackestones, of supposed Berriasian age (Barale, 2014; Barale *et al*., 2016). In the Mont Chajol sector, the Middle–Upper Jurassic succession is formed by micritic limestones with *Saccocoma* and ammonites, attributed to a more pelagic environment with respect to the carbonates of the adjoining sectors. They locally contain beds of oolitic grainstones, interpreted as resedimented deposits.

METHODS

Petrographic studies on 70 uncovered thin sections (30 μm thick) were carried out by optical microscopy and cathodoluminescence (CL) with the aim of distinguishing different dolomite generations. CL observations were carried out on polished thin sections using CITL 8200 mk3 equipment (operating conditions of about 17 kV and 400 μA). In situ quantitative microprobe analyses were performed on carbon-coated thin sections with an energy dispersive x-ray spectroscopy (EDS) Energy 200 system and a Pentafet detector (Oxford Instruments) associated with a Cambridge Stereoscan S-360 scanning electron microscope (SEM). The operating conditions were 15 kV of accelerating voltage, around 1 nA of probe current, and 50 seconds of counting time. SEM–EDS quantitative data (spot size: 2 μm) were acquired and processed using the Microanalysis Suite Issue 12, INCA Suite version 4.01; Structure Probe, Inc. (SPI) natural mineral standards were used to calibrate the raw data; the RoPhiZeta correction (Pouchou and Pichoir, 1988) was applied. Analytical statistical errors ∑ on atomic weight percent are 0.08 for Mg and Fe and 0.13 for Ca. Carbon and oxygen isotopic compositions of the carbonates were measured partly at the Stable Isotope Laboratory of the ETH Geological Institute, Zurich, Switzerland (using a Thermo Fisher Scientific GasBench II coupled to a Delta V mass spectrometer as described in Bretenbach and Bernasconi (2011)), and partly at the MARUM Stable Isotope Laboratory, Bremen, Germany (using a Finnigan MAT 252 mass spectrometer and following the standard method of McCrea (1950)). In both cases, the oxygen isotope composition of dolomite was calculated using the fractionation factor of Rosenbaum and Sheppard (1986). The isotopic ratios for carbon and oxygen are expressed as $\delta^{13}C$ and $\delta^{18}O$ per mil values relative to the VPDB (Vienna Pee Dee Belemnite) standard (precision ±0.05‰). Fluid inclusion petrography has been studied on bi-polished thin sections (80 μm thick). Microthermometry of primary fluid inclusion assemblages on dolomite and calcite was performed using a Linkam THMSG600 heating–freezing stage coupled with an Olympus polarizing microscope (100× objective), using the standard method described by Goldstein and Reynolds (1994). Crystal size classes used in dolomite description are those proposed by Folk (1962).

DOLOSTONE MAIN FEATURES

Geometry, distribution and structures of the dolomitized bodies

Dolomitization affects the whole thickness of the Middle Triassic carbonates and of the overlying Garbella Limestone for a total thickness of about 400–500 m (Fig. 3). Sediments overlying the Garbella Limestone are not dolomitized, but they locally contain clasts of dolomitized rocks, as described below. In the study area, the Triassic–Jurassic succession shows different modes and degrees of dolomitization (Fig. 2). Dolomite occurs both as a replacement phase and as a void-filling cement. The term "dolomitization degree" is used here as a qualitative evaluation, considering the volumetric abundance of dolomite with respect to the host rock and the degree of overprint on the primary fabric. The highest degree is observed in a belt with a rough NW–SE orientation, about 2 km wide and 8–10 km long, extending from Punta Bussaia to the eastern side of the Sabbione Valley, and in the Mont Chajol–Mont Agnelet–Mont Paracouerte sector. In these areas dolomitization widely affects a great part of the Provençal carbonate succession (Fig. 4), and fabric-destructive facies are common, as well as breccias, dissolution cavities, and tightly spaced vein networks. Outside these areas, the dolomitization degree decreases: fabric-retentive facies prevail, whereas the fabric-destructive ones are limited to isolated masses of decimetre to metre size. Breccias and dissolution cavities are rare, and vein networks are more spaced. Similar dolomitization phenomena, though less intense, locally affect the Middle–Upper Jurassic and Berriasian limestones in other sectors of the Provençal Domain (southern side of Argentera Massif and Nice Arc: Dardeau and Bulard, 1978; Malaroda, 1999; Barale, 2014) (Fig. 5). In the Jurassic part of the succession, dolomitization gave rise mainly to light-coloured, intensely dolomitized bodies that are commonly irregularly shaped, vary in size from some decimetres to some hundred metres (Figs. 4, 6A), and show randomly oriented boundaries with the encasing limestones. Conversely, in the Triassic part of the succession, well exposed in the Mont Chajol–Mont Agnelet-Mont Paracouerte area, dark dolomite-cemented breccias prevail (Fig. 7) and light, pervasively dolomitized bodies are commonly limited to smaller masses, decimetre-thick and a few metres wide at most. They generally crosscut the host-rock bedding

(Figs. 8A and C) but some stratabound occurences have also been observed (Figs. 6B and 8B).The transition between completely dolomitized and undolomitized or poorly dolomitized rock volumes is commonly very sharp and takes place in a few centimetres (Figs. 6B, 8A and C). In the Garbella Limestone, bedding-parallel burial stylolites systematically cut through dolomite crystals and veins (Fig. 9A).

Dolomitization textures

Partially dolomitized limestones constitute the greatest volume of the dolomitized rocks in the study area. Four main types of partial-dolomitization fabrics can be distinguished:

- Matrix-selective. Dolomitization of the matrix can be either partial or complete, but it affects the grains very marginally.
- Grain-selective. Dolomitization affects only the grains, or a particular kind of grain. This kind of selective dolomitization is commonly observed in the coarse-grained facies of the Garbella Limestone, where it typically affects large bioclasts in rudstones and boundstones (Fig. 9B) or ooids in oolitic grainstones.
- Non-selective. The host rock is partially replaced by medium to coarsely crystalline dolomite growing indifferently on the grains and on the matrix/cement of the rock (Fig.10A).
- Veined limestones. Dolomitization develops along a vein network, with euhedral dolomite crystals spreading from the veins and substituting the surrounding rock (Fig. 10B). Locally, a higher vein density is present within subvertical, centimetre- to decimetre-wide, tabular rock volumes (Fig. 10C). Veins are 200 μm to 2 mm thick on average and show a thin inner part (100–200 μm), composed of finely to medium crystalline turbid dolomite and a thicker outer part (100–1000 μm) composed of outward growing, coarse to very coarsely crystalline dolomite crystals (Fig. 10D and E). The latter grow as a replacement of the rock constituting the vein walls. Dolomite veins do not show any preferential orientation. These veins can be clearly distinguished from those related to Alpine structural associations, which commonly bear a large number of tectonic calcite veins both in fold-related settings and fracture networks. Furthermore, dolomite veins are systematically cut by a recurrent N–NE-striking system of tectonic calcite veins, widespread in the study area. A few isolated crystals can also occur in the host rock, far from the veins, but the majority of dolomite grows directly from the veins, and the portions of the host-rock away from the veins are generally undolomitized. This

kind of dolomitization is typically observed in the mudstone–wackestone beds of the Garbella Limestone.

Completely dolomitized rocks occur mainly in the Jurassic succession as discrete masses, some metres to some tens of metres wide, randomly distributed within partially dolomitized limestones. The two principal types are whitish, fine to medium crystalline dolostones and white, sucrosic, coarsely to very coarsely crystalline dolostones. Primary rock fabrics are commonly obliterated, although in some cases ghosts of the original fabric are still recognizable.

Breccias

Breccias form bodies with complex geometries, consisting of mainly tabular parts, at a high angle with respect to bedding, a few centimetres to some metres wide, which can be followed vertically for up to some tens of metres, and generally thinner bodies that develop along bedding planes in the host rock (Figs. 7, 11A and B). Four main breccia types have been recognized and are described below using the descriptive, non-genetic classification of carbonate breccias by Morrow (1982).

- Type-1 are clast-supported, monomictic breccias with clasts of undolomitized rocks , with the same lithology as the host rock. Clasts are generally angular and millimetre- to centimetre-sized and locally show a jigsaw-puzzle arrangement (Fig. 11C). Voids are cemented by millimetre- to centimetre-thick rims of white, coarsely to very coarsely crystalline dolomite, followed by calcite. Locally, internal sediments are present, either predating or postdating dolomite cements (Fig. 11D). Detailed petrographic and cathodoluminescence analyses show important differences and asymmetries in the stratigraphy of cement rims around different clasts or on different sides of the same clast. A gradual transition between veined limestones and type-1 breccias is commonly observed, occurring by a progressive increase of clast displacement resulting in the formation of centimetre-wide voids filled with coarse to very coarse dolomite cement (Fig. 11E). Clasts within these breccias are locally crossed by millimetre-thick dolomite veins and thus consist of veined limestones (Fig. 11F). Type-1 breccias can be either crackle, mosaic, or rubble packbreccias (sensu Morrow, 1982).
- Type-2 are clast-supported, monomictic breccias with clasts of homogeneous, medium to coarsely crystalline dolostones, generally showing the same lithology as the host rock. They are centimetre- to decimetre-sized, and sub-rounded to angular in shape (Fig.11G). Voids between the clasts are cemented by a millimetre- to centimetre-thick rim of coarsely to very coarsely crystalline white dolomite, with calcite plugging the

remaining pores. These breccias are mostly mosaic to rubble packbreccias or, less commonly, rubble floatbreccias (sensu Morrow, 1982).

- Type-3 are polymictic, clast-supported breccias with centimetre- to decimetre-sized, angular to subrounded clasts composed of coarsely-crystalline dolostones, limestones, and partially dolomitized limestones (including clasts of limestones with dolomite veins clearly truncated at the clast edge) (Fig. 11H). Voids between clasts are filled up with a micritic matrix containing sand-sized clasts of the same lithologies as larger clasts. Type-3 breccias are mostly rubble packbreccias (sensu Morrow, 1982).
- Type-4 are clast-supported monomictic breccias, mostly composed of millimetre- to centimetre-long and millimetre-wide plate-like clasts (rubble floatbreccias sensu Morrow, 1982) (Fig. 12A). The clasts show a constant and particular fabric: a central part of finely to medium crystalline dolomite is surrounded on the two sides by coarse crystals of white dolomite growing outward from the central part. The shape of the clasts is angular, and their outline mostly coincides with the dolomite crystal faces. Voids between clasts are cemented by dark-grey, sparry calcite (Fig. 12A). Type-4 breccias are commonly found within veined limestone, as tabular bodies bordered by veins, forming a high angle with the host-rock bedding (Fig. 12B).

Cavities

Irregularly shaped cavities are frequent in the dolomitized rocks and are commonly millimetre- to centimetre-sized, but they can locally reach several decimetres in diameter (Fig. 13A). Cavities are commonly fringed by an isopachous rim of coarsely crystalline dolomite cement, locally showing a jagged outline (Fig. 13B), followed by sparry calcite. They host internal sediments, giving rise in some cases to geopetal structures (Fig. 13C). Sediments are mainly silt-sized, locally passing to very fine and fine grained sands (up to 200 μm in diameter), and are commonly laminated (Fig. 13D and E). They generally consist of calcite, but they locally contain fragments of coarsely crystalline dolomite crystals. Laminae are some hundred micrometres to a few millimetres in thickness and show a normal grading. Locally, these sediments are dolomitized and appear as a homogeneous mosaic of anhedral to subhedral, finely to medium crystalline dolomite crystals. In some large cavities, a first layer of dolomitized sediment is followed by a second one of undolomitized sediment (Fig. 13E). In most cases internal sediments are deposited above dolomite cement rims and are followed by calcite cement (Fig. 13C). Locally, however, sediments can occur in any position, from below the first cement generation to above the last one.(e.g. Fig. 13D). Cavity fills also contain clasts which are represented by fragments of the wall-rock or of early cement rims (Fig. 13A and E). A particular kind of cavities occurs in veined limestones and are entirely bordered by veins, giving rise to a boxwork fabric (Fig. 13F). A sparry calcite cement plugs these cavities.

Both partially and completely dolomitized rocks show a very low porosity, quantifiable as less than 2%. Cavities and fractures are completely occluded by cement, and no significant inter-crystalline porosity is present in dolostones.

Reworked dolomite

In the Colle di Tenda area, the Nummulitic Limestone directly overlies the dolomitized Garbella Limestone, and starts with a metre-thick bed of clast-supported conglomerate with decimetre-sized clasts of limestones and coarsely crystalline dolostones (Carraro *et al*., 1970; Campredon, 1977), with *Gastrochaenolites* bivalve borings (Fig. 14). The conglomerate is followed by a succession of decimetre-thick, normally graded beds, made up of conglomerates to arenites, whose clasts and grains consist of dolomitic rocks and fragments of single dolomite crystals with petrographic and cathodoluminescence features comparable to the underlying dolomitized carbonates. Similar dolostone clasts, have been recently found also in Cretaceous sediments of the adjoining Dauphinois succession, in particular in Valanginian–Hauterivian p.p. pebbly mudstones locally draping the Caire Porcera palaeomargin (Lausa Limestone; Barale, 2014; Barale *et al*., 2016).

PETROGRAPHY, CATHODOLUMINESCENCE, AND ELECTRON MICROSCOPY

Petrographic analysis of the dolomitized rocks allowed different mineralogical phases related or subsequent to the dolomitization event to be distinguished. For dolomite phases, the morphological classification of Sibley and Gregg (1987) has been utilized. Four dolomite types have been recognized:

- Dol1. Finely to medium crystalline planar-s dolomite. It has a turbid appearance in thin section due to the abundance of small fluid and solid inclusions. Dol1 occurs both as a cement in the inner parts of dolomite veins (Figs. 10D, E), and as replacement phase in all kinds of host limestones throughout the succession (Fig. 15A). Dol1 commonly gives rise to homogeneous, beige-coloured dolostones that do not preserve any relict primary depositional fabric. Dol1 shows a dull to moderate, blotchy, orange–red CL. This CL pattern invariably characterizes Dol1 throughout the study area.
- Dol2. Coarsely to very coarsely crystalline planar-e dolomite. It occurs as a replacement phase, commonly in micritic facies of the Garbella Limestone, and forms euhedral

crystals, up to 1–2 mm in size (Fig. 15B), showing unit extinction under crossed polars. Crystals generally show a large inner portion with abundant micrometre-sized calcite inclusions representing portions of the replaced sediment and a clearer thin outer rim, some tens of micrometres thick, almost devoid of solid inclusions. Dol2 is commonly non-luminescent in CL. Only locally does the external part of the crystals have some hairline zones with moderate to bright red–orange CL.

Dol3. Non-planar, coarsely to extremely coarsely crystalline (500–5000 μm) dolomite. It has curved crystal faces and a marked sweeping extinction (Fig. 15C). In the outer part of the crystals, the alternation of more and less inclusion-rich bands defines a zoning which defines different growth stages. It occurs both as cement (saddle dolomite) and as replacive dolomite. The former gives rise to millimetre-thick rims fringing cavity walls and breccia clasts (Fig. 15B). Commonly, cavity-filling saddle dolomite has a cloudy inner part and a clear outer rim some tens of micrometres thick. Replacive Dol3 crystals typically grow from the veins outward (Fig. 10D and E) but also occur in the host limestone as isolated crystals, euhedral to subhedral and up to 2–3 mm in size. In some cases, Dol3 can completely replace the host rock, giving rise to a coarsely to very coarsely crystalline, sucrosic dolostone. In this case, it forms a mosaic of subhedral to anhedral crystals, 500–1000 μm in size on average, with larger crystals up to 4 mm in size. Larger crystals locally preserve ghosts of primary fabrics, evidenced by alignments of minute calcite inclusions. Dol3 crystals have, as a general trend, a thick inner part with a homogeneous, dull to moderate red–orange luminescence, analogous to that of Dol1. This zone is followed by a thick non-luminescent zone locally showing hairline, moderately to brightly luminescent orange zones. The outer part of the crystals has a moderate to bright luminescence with a well-defined zonation, resulting from the alternation of red–orange, orange, and non-luminescent zones (Fig. 16A and B).

Dol4. Fibrous dolomite cement, forming elongated, blade- to fan-shaped crystals with rhombic terminations, up to 7–8 mm long and 1–2 mm wide, with the long axis perpendicular to the substrate. Crystals show sweeping extinction with diverging optical axes of the fibres (fascicular-optic; e.g., Richter *et al.*, 2011) (Fig. 15D). Dol4 is common as breccia and cavity cement in the Mont Chajol sector, whereas it has not been observed in other sectors. Dol4 has a moderate orange or red–orange CL, with a well-defined zonation in the outer part of the crystals, deriving from the alternation of zones with slightly different CL colour or intensity.

SEM–EDS analyses show that all the above-described phases are non-ferroan, high-Ca calcium dolomites (*sensu* Jones and Luth, 2002). The $CaCO_3$ content is 57–59 mol% in Dol1, 54–56 mol% in Dol2, 56–59 mol% in Dol3, and 56–60 mol% in Dol4.

Calcite (Cc1) represents the last phase of void cementation throughout the study area. It is a coarsely to extremely coarsely crystalline sparry calcite (Fig. 15C), forming anhedral crystals that commonly show polysynthetic twinning. It is generally limpid in thin section, whereas on the hand sample the colour is variable, from white to dark-grey or blackish (Fig. 13A and F); the latter smells like oil when crushed. Cc1 shows a dull to moderate yellow–orange to greenish yellow CL with a local zonation resulting from the alternation of luminescent and non-luminescent zones.

Dol1, Dol3, and Cc1 are the most commonly observed phases and are widespread throughout the study area. Dol1 predates Dol3 . This can be clearly observed in cavities, where Dol3 saddle dolomite cement grows on the Dol1 replacement dolomite commonly representing the cavity wall, and in veins, where the inner part, made up of Dol1, is overgrown by outward-growing Dol3 crystals (Fig. 10D and E). Cc1 is the last phase of void filling, ubiquitously postdating Dol3 cement. Dol2 has a wide distribution in the study area, but it seems to be limited to fine-grained host rocks (mudstones and wackestones), whereas Dol1 and Dol3 are common replacement phases in all types of rocks. Dol4 cement has only been observed in samples coming from the Mont Chajol sector.

STABLE ISOTOPE GEOCHEMISTRY

Twenty dolomite samples were measured to determine their $\delta^{18}O$ and $\delta^{13}C$ isotopic values. Samples consisted of Dol1 replacement dolomite, Dol3 saddle dolomite cement, and Dol4 cement. The data obtained are similar for all dolomite types (Fig. 17): $\delta^{18}O$ values range from –2.00 to –11.03‰ VPDB, and the majority of them range between –4 and –7‰ VPDB, whereas $\delta^{13}C$ values mostly range between +1 and +2‰ VPDB. Two samples of Cc1 calcite were also measured: they show negative $\delta^{18}O$ values (–7.73 and –7.24‰ VPDB), whereas $\delta^{13}C$ values are –2.10 and +0.50‰ VPDB, respectively. Lastly, eight samples of undolomitized Triassic and Jurassic carbonates have been measured: they show $\delta^{18}O$ values between –4.21 and –1.63‰ VPDB and $\delta^{13}C$ values between –0.53 and +2.53‰ VPDB.

FLUID INCLUSION ANALYSIS

More than 100 fluid inclusions from 8 double-polished sections have been measured to find their homogenization temperatures with a standard heating method (Goldstein and Reynolds, 1994).

Primary fluid inclusions of useful size for microthermometry (i.e. greater than than 2 μm in diameter; Goldstein and Reynolds, 1994) were found in the clear, outer rim of Dol3 and Dol4. The distribution of these inclusions along growth zones documents their primary origin. They are two-phase inclusions, liquid-rich with a vapour bubble, with irregular shapes, varying in size from 2–3 up to 10 μm. No evidence of stretching of either crystals or inclusions has been noted. Primary fluid inclusions show a relatively tight distribution of homogenization temperatures, ranging from 170 to 240 °C in Dol3 (highest frequency around 200 °C) and from 190 to 260 °C in Dol4 (highest frequency around 230 °C) (Fig. 18). Larger fluid inclusions in Dol3 were also utilized for low-temperature runs to infer the fluid composition. The only recognizable phase observed was ice, with final melting temperatures between –20 and –24 °C, whereas the eutectic temperatures were not clearly determinable. The measured final melting temperatures of ice are lower than the eutectic temperature of the H_2O–NaCl system (–21.2 °C), thus pointing to a more complex system with cations other than Na^+, possibly Ca^{2+} and Mg^{2+}. Assuming a NaCl–$CaCl_2$–$MgCl_2$–H_2O system (eutectic temperature -57°C; Shepherd *et al.*, 1985) as a possible approximation for the fluid inclusion composition, the observed final melting temperatures indicate a highly saline fluid with an approximate salinity of 20–23% $CaCl_2$ equivalent (salinity is expressed in $CaCl_2$ equivalent following Bakker and Baumgartner, 2012).

DISCUSSION

Age of dolomitization

On the basis of the stratigraphic relationships described in this paper, the timing of dolomite formation is well constrained. Dolomitization has to be younger than the youngest dolomitized rocks, which are the top interval of the Garbella Limestone, dated to the Berriasian. On the other hand, dolomitization has to be older than the oldest sediments containing dolomite clasts. Clasts derived from erosion of the dolomitized Garbella Limestone are present in Valanginian–Hauterivian p.p. sediments locally draping the Caire Porcera palaeomargin (Barale, 2014). The presence of dolostone clasts in Valanginian–Hauterivian p.p. sediments thus indicates that dolomitization cannot be younger than Valanginian. To summarize, the studied hydrothermal dolomitization occurred in the earliest Cretaceous, probably in the latest Berriasian–Valanginian interval.

Burial conditions during dolomitization

In order to reconstruct the diagenetic environment of dolomitization, the burial history of the host rocks has to be considered. As concluded above, dolomitization took place in the earliest Cretaceous (latest Berriasian–Valanginian). Lower Cretaceous sediments are very thin or completely missing in the study area, more likely due to condensation and non-deposition than to subsequent erosion. The Lower Cretaceous Provençal succession is in fact condensed throughout the Maritime Alps (e.g., Lanteaume, 1968, 1990; Decarlis & Lualdi, 2008; Barale *et al.*, 2013b). Thus, in the latest Berriasian–Valanginian, the top of the Garbella Limestone should have been very close to the seafloor. This is confirmed by the absence of compactional features (e.g., concave-convex grain contacts) in dolomitized ooid grainstone beds of the Garbella Limestone, documenting that dolomitization occurred before the onset of burial-related compaction of sediments (Fig. 10A). Moreover, in the Garbella Limestone, dolomite veins are locally cut by bedding-parallel stylolites, again indicating that dolomitization occurred before the deep burial of the succession (Fig. 9A).

Contextually, the lower part of the Middle Triassic carbonates should have been buried to a depth of 400–500 m, corresponding to the cumulative thickness of the Garbella Limestone and the Triassic carbonates themselves. For this reason, the temperature of the host rock at the time of the dolomitization event should have been very low, close to seawater temperature (which was around 35 °C at the surface in Early Cretaceous low-latitude seas: Schouten *et al.*, 2003, Littler *et al.*, 2011) in the upper part of the dolomitized succession and slightly higher in the lower part. On the other hand, microthermometric data indicate that dolomitizing fluids were significantly hotter (180–240 °C), and thus they can be properly considered as hydrothermal fluids (sensu Machel and Lonnee, 2002; Machel, 2004; Davies and Smith, 2006).

Hydrothermal minerals

Among the different mineral phases described above, Dol1, Dol2, and Dol3 dolomites and Cc1 calcite are the most important ones, as they are ubiquitous in the studied rocks. Dol4 is present only in a limited sector (Mont Chajol). Dol1 and Dol2 are both replacement phases, although showing very different features. It is not clear which factors controlled the development of Dol1 rather than Dol2. The host-rock lithology might have played some role, as Dol2 has been observed almost exclusively in micritic rocks whereas Dol1 replaces all kinds of host limestones. It is possible that partly lithified, and thus less porous and permeable, micritic host rock impeded an efficient flux of dolomitizing fluids thus allowing a smaller number of dolomite crystals to nucleate, and promoting their non-competitive growth to larger sizes, whereas in more porous host rocks, e.g. non-cemented carbonate sands, the competitive growth of numerous crystals generally resulted in a small crystal size. Dol3 also occurs as a replacement phase. Comparable oxygen isotope values of Dol1 and Dol3, and the lack of fluid inclusion microthermometric data for Dol1, do not allow reliable hypotheses to be made on the factors controlling the development of Dol3 rather than Dol1.

Dol4 fascicular-optic dolomite is only present in the Mont Chajol area, where it forms thick cement rims in breccias, cavities, and veins, analogously to Dol3 saddle dolomite. Stable isotope and microthermometric data do not show clear differences between the fluids which precipitated Dol4 and those which precipitated Dol3 saddle dolomite, and thus do not allow us to understand which factors locally favoured the precipitation of Dol4 instead of Dol3.

Cc1 is the last phase of cement precipitation which plugs the remaining pores. Many examples are reported in which calcite is closely associated with dolomite as a late-stage hydrothermal phase precipitating at a lower temperature (e.g. Lavoie *et al*., 2005; López-Horgue *et al*., 2010; Sharp *et al*., 2010). The change from dolomite to calcite precipitation has been related to a late-stage calcite saturation in the fluid as a result of Mg exhaustion or, alternatively, to a switch of hydrothermal fluids from dolomite to calcite supersaturation due to a drop in temperature.

Rock fabrics

The whole Middle Triassic to Berriasian succession, several hundreds of metres thick, is affected by dolomitization. Nevertheless, striking differences exist in the response of host rocks to the flow of dolomitizing fluids: in Triassic carbonates, breccias prevail and dolomitized bodies are smaller and scattered, whereas in the Middle Jurassic–Berriasian limestones a pervasive dolomitization (partial or complete) of the host limestones occurs (Fig. 3).

Partial versus complete dolomitization

Partially dolomitized rocks are volumetrically the most important form of dolomitization, and are affected by non-selective or selective dolomitization. The latter affects from place to place either the matrix or the grains, and seems to be controlled by a number of factors: crystal size of the calcareous precursor (micrite vs. monocrystalline echinoderm fragments), mineralogy of the calcareous precursor (aragonite vs. calcite), early diagenetic processes such as cementation and neomorphism modifying, respectively, permeability and chemical stability of grains (e.g., Murray and Lucia, 1967; Sibley, 1982; Bullen and Sibley, 1984; Sibley and Gregg, 1987). The features of the sediment resulting from either depositional or early diagenetic processes interplayed with the chemical characteristics of dolomitizing fluids (e.g., saturation) which, in turn, could vary both in space and time resulting in a complex spectrum of dolomitization modes.

Veined limestones represent a common type of partially dolomitized rocks, and are commonly developed in mudstones or wackestones, whereas matrix-poor, grainy textures show a more diffuse dolomitization. Tight, partly litified, mud-supported sediments possibly did not allow a diffuse, pore-controlled, fluid flow, but only a focused flow through a network of fractures, and dolomite formation was limited to vein cement and substitution of the host rock adjacent to the vein walls. Completely dolomitized bodies are decimetre- to decametre-sized, show an irregular shape and are randomly distributed in the sedimentary succession and commonly discordant with the bedding. Only locally, in Middle Triassic carbonates, thin, laterally discontinuous, shale beds acted as minor barriers to the fluid flow and caused them to expand laterally, giving rise to decimetre- to metre-sized, stratabound dolomitized bodies. The factors controlling the distribution of dolomitized bodies probably lie in the intensity of the fluid flow and in the total volume of hydrothermal fluids circulating through the rock. These factors could be controlled in turn by the distance from the main fluid-flow pathways. Dolomitized bodies locally show a very sharp dolomitization front (Figs 6B, 8A and C), possibly corresponding to the margins of highly fractured rock volumes acting as fluid conduits.

Cavities

The irregular shapes of the cavities, generally with smooth and rounded edges, and their relatively large dimensions indicate that they formed as a consequence of dissolution processes. Moreover, the incongruent cement stratigraphy on different parts of cavity walls and around clasts, as well as the presence of cement clasts, indicate that cavity opening was a polyphase process. Phases of cavity enlargement by dissolution and subsequent cement precipitation on cavity walls likely alternated with phases of fracturing affecting both the cavity walls and the early cement rims grown on them (Figs. 11D, 13C, D and E, 19). Cavities commonly host laminated internal sediments. The relationships among the internal sediments and hydrothermal cements, in particular saddle dolomite, clearly document that the sediment deposition occurred indifferently before, after, or between different phases of cement precipitation (Fig. 19). This, together with the fact that internal sediments are locally dolomitized, indicates that sediment deposition occurred when the hydrothermal system was still active. As to the origin of the sediments, there are two possibilities. The first hypothesis is that sediments originated within the hydrothermal system, deriving both from the erosion of cavity and fracture walls during the flow of the hydrothermal fluids, and from mobilization of still unconsolidated levels of the sedimentary succession. The second hypothesis, conversely, is that they derived from infiltration of loose sediment from the seafloor. Internal sediments are present both in cavities hosted in the Garbella Limestone, whose upper portion was close to the seafloor at the time of dolomitization, and in the Middle Triassic carbonates (Monte Chiamossero, Mont Agnelet), which during and after the dolomitization event were separated from the seafloor by the entire thickness of the Jurassic succession (over 200 m). This considerable depth value does not rule out, in principle, the possibility of a sediment infiltration from the seafloor. In fact, sediment infiltration has been documented in cavity networks down to a depth of 300 m from the seafloor (Aranburu *et al*., 2002). However, internal sediments locally contain sand-sized dolomite clasts that have been recognized as fragments of cavity-wall cements. This indicates that at least a part of the sediments has an intra-system provenance, even though a mixing of intra- and extra-system sediments cannot be excluded.

Breccias

Breccias are characterized by some common features:

- the angular shape and the jigsaw puzzle arrangement of clasts;
- the apparent floating fabric of clasts, clearly due to dilation;
- the high-angle orientation of the tabular breccia bodies with respect to host-rock bedding.

These features point to hydrofracturing processes related to mainly vertical fluxes of overpressured fluids (e.g. Phillips, 1972; Ohle 1985). Most breccias are monomictic, with clasts of the same lithology as the encasing rock. This documents that they derive from in situ disruption of the encasing rock, with a limited or no transport at all of the clasts. Conversely, the polymictic nature of type-3 breccias implicates some sort of clast transport, even though it is not known over what distance. Also, the fine-grained matrix locally present in type-3 breccias likely derived from transport and deposition of loose sediments. As to the origin of these sediments, the same considerations as for internal sediments in cavities are valid. Rounded breccias clasts formed by partial dissolution of the clast edges (cf. Iannace *et al*., 2012), as other rounding mechanisms, such as a prolonged transport, can be confidently ruled out.

Type-4 breccias deserve a separate discussion, because their unusual composition and fabric reflect a particular genetic mechanism. The shape and structure of the clasts strongly resemble those of the dolomite veins crosscutting the host limestones, and thus clasts reasonably represent fragments of such veins. Locally, on the outcrop, a lateral transition from veined limestones to type-4 breccias has been actually observed via a series of intermediate facies with increasing host-rock dissolution and disruption of the vein network. These breccias are related to a dissolution process, locally affecting veined limestones. The steps of type-4 breccia formation can be summarized as follows (Fig. 20):

- The host limestone is crossed by a network of thin fractures. Dolomitizing fluids flow through this crack system, resulting in dolomite cementation of the fractures and dolomitization of their walls ;
- a local but complete dissolution of the host limestone occurs, leaving a fragile network of isolated dolomite veins (boxwork fabric);
- the vein network collapses, forming clasts of vein material;
- clasts are cemented by sparry calcite.

In conclusion, type-1, -2, and -3 breccias originated through hydrofracturing processes and show only local evidence of dissolution (rounded clasts). On the contrary, type-4 breccias are only indirectly connected to hydrofracturing, but document strong dissolution of veined limestones.

Characters and origin of dolomitizing fluids

The isotopic composition of hydrothermal dolomite shows slightly positive $\delta^{13}C$ values, mostly between 1 and 2‰ VPDB, and negative $\delta^{18}O$ values, varying from –2 to –11‰ VPDB. The $\delta^{13}C$ values overlap with values from Triassic and Jurassic sediments not affected by hydrothermal dolomitization and are in the range of carbonates precipitated from seawater (e.g. Podlaha *et al*., 1998; Nunn and Price 2010). This probably indicates that the host rock had a buffering effect on the carbon-isotope composition of the dolomite, as is commonly observed in dolomitization processes (e.g. Hoefs, 2009). Conversely, the $\delta^{18}O$ values of hydrothermal dolomite differ significantly from the values of Triassic and Jurassic sediments not affected by hydrothermal dolomitization, being markedly more negative. Calculation of the isotopic composition of the parent fluids was made by combining the $\delta^{18}O$ data measured on hydrothermal dolomite with the precipitation temperature obtained in the very same spots by fluid inclusion microthermometry (this was possible in very coarse, Dol3 and Dol4 cements). According to the fractionation equation of Land (1985), the combination of these data indicates highly ^{18}O-enriched dolomitizing fluids, ranging from about +9 and +12‰ Standard Mean Ocean Water (SMOW). The final melting temperature of fluid inclusions indicates that dolomitizing fluids were highly saline fluids characterized by a complex composition that could be represented by the $NaCl–CaCl_2–MgCl_2–H_2O$ system and an approximate salinity of 20–23% $CaCl_2$ equivalent. Basinal and evaporitic brines are commonly indicated as probable sources of highly saline fluids in hydrothermal systems (e.g. Davies and Smith, 2006; López-Horgue *et al*., 2010; Shah *et al*., 2012; Lapponi *et al*., 2014). Moreover, such brines are highly ^{18}O-enriched, as are waters deriving from salt dissolution or gypsum dehydration (Hitchon and Friedman, 1969; Knauth and Beeunas, 1986). In the study area,basinal brines could have entered the hydrothermal system only from the adjoining Dauphinois succession, that, however, was too thin (a few hundred metres; Carraro *et al.*, 1970; Barale *et al*., 2016) to provide large amounts of fluids. For this reason, the most important source of fluids was likely to be seawater, whose original composition still had to be strongly modified to produce the highly saline, ^{18}O-enriched dolomitizing fluids. The interaction with evaporite intervals is commonly invoked to explain the high salinity and $\delta^{18}O$ values of dolomitizing fluids (e.g. López-Horgue *et al*., 2010; Shah *et al*., 2012; Lapponi *et al*., 2014; Geske et al., 2015). Upper Triassic evaporites are present in the stratigraphic succession of the Maritime Alps (Lanteaume, 1968; Carraro *et al*., 1970). This evaporite interval represents a preferential detachment horizon in the stratigraphic succession and it is not cropping out at present in the study area due to tectonic lamination, even though masses of Upper Triassic evaporites are locally present in the subsurface (Colle di Tenda tunnel; Ivaldi *et al*, 1998; Cavinato *et al*., 2006). However, the original thickness of Upper Triassic evaporites is unknown, and therefore it is not possible to establish if this interval could have played a significative role in modifying the composition of dolomitizing fluids. Another possible mechanism for increasing the salinity of fluids and enriching them in ^{18}O is the interaction with silicate minerals of siliciclastic and crystalline rocks (Clayton *et al*., 1966; Land and Prezbindowski, 1981; Hitchon *et al*., 1990). As mentioned above, high precipitation temperatures document that dolomitizing fluids were involved in a deep hydrothermal circulation. Considering the extreme reduction of the Middle Triassic–Jurassic sedimentary succession in this area (not more than 400–500 m), it is very likely that fluids interacted with Permian–Lower Triassic siliciclastic rocks and with the crystalline rocks of the basement, currently exposed in the Argentera Massif (Fig. 21). This interaction possibly accounts for the enrichment in ^{18}O and the increase in salinity of the dolomitizing fluids. Actually, the less ^{18}O-enriched values of the dolomitizing fluids, calculated from the most ^{18}O-depleted dolomites, can be considered as the most representative of the fluids. The less depleted values of the dolomite could conversely be the result of important interactions between dolomitizing fluids and host rocks and as such not suitable to calculate the isotopic composition of dolomitizing fluids. A reasonable value for the latter therefore is around +8‰ SMOW or even lower and hence perfectly consistent with waters that have strongly interacted with silicate-rich basement rocks (e.g., Haeri-Ardakani et al., 2013a, b).

Processes and features of the hydrothermal system

Temperatures obtained for dolomitizing fluids are anomalously high if compared to the low temperatures inferred for the dolomitized rocks from their shallow burial depth. In the study area there is no evidence of magmatic activity in the Mesozoic, which could have represented a heat source for the fluids. Therefore, the high temperature of the fluids documents a very deep hydrothermal circulation related to deep-rooted fault systems (Fig. 21)., as commonly hypothesized for hydrothermal systems related to high-temperature and shallow-burial dolomitization (e.g. Davies and Smith, 2006; López-Horgue *et al*., 2010; Shah *et al*., 2012). In the study case, the measured homogenization temperatures of around 200° C would imply, assuming a normal geothermal gradient of about 30 °C/km, a circulation depth of at least 7 km. However, in extensional continental margins, crustal thinning is associated with anomalously high geothermal gradients (up to 80 °C/Km; Goldberg and Leyreloup, 1990; Vacherat *et al*., 2014), which moreover can persist for a few tens of Myr after the end of rifting (Vacherat *et al*., 2014). Such high gradients would significantly reduce the maximum depth of the hydrothermal system. The ubiquitous association of dolomitized bodies with vein networks and the common presence of dolomite-cemented, subvertical, tabular breccia bodies indicate that dolomitization was related to the circulation of fluids through high-angle faults and the related fracture systems. In this sense, the hydrothermal system was controlled by fracture porosity (sensu Choquette and Pray, 1970) related to faults and fracture systems, which exerted the most important control on the permeability of the host carbonates (e.g, Iriarte *et al*., 2012). Intrinsic porosity variations among the different rock facies had only a minor control on fluid circulation, possibly influencing the distribution of dolomitization only at the very local scale and away from the major fluid-flow pathways, where the fluid flow was less intense and pervasive. Dolomite both precipitated along fault and fracture systems and replaced, partially or completely, non-fractured portions of carbonate rocks. This indicates that part of the host carbonates were still permeable enough to allow a diffuse flux of dolomitizing fluids. At the time of dolomitization, the Triassic and Jurassic parts of the succession differed in several aspects, such as lithofacies, composition, permeability, coherence, and burial depth, which altogether influenced the modes of dolomitization. The Triassic sediments were mainly fine-grained limestones and dolostones, and evenly bedded because of thin shale partings. Moreover, their porosity was reduced by the overburden of the overlying sediment column. Therefore, on the whole, they were less permeable and compositionally less prone to dolomite replacement. Conversely, the Jurassic succession was more shallowly buried and in part composed of coarse-grained, mud-poor carbonate sediments. Consequently, pervasive dolomitization was favoured in the more permeable and shallower Jurassic limestones, whereas deeper in the rock column, hydraulic fracturing processes prevailed with the development of a network of breccia conduits.

The random 3D orientation of vein networks and the common presence of hydrofracturing-related breccias indicate the importance of hydrofracturing processes in the evolution of the hydrothermal system. Hydrofracturing was related to the abrupt expulsion of overpressured fluids along main fluid-flow pathways, likely represented by high-angle faults and the related subvertical breccia bodies and fracture systems. Polyphase breccias point to multiple events of hydrofracturing, in turn related to cyclic expulsion of overpressured fluids. Cyclic fluid expulsion through fault systems can be explained by the so-called fault–valve model (Ramsay, 1980; Sibson, 1987, 1992), which involves alternating phases of fluid accumulation and expulsion. It is thus probable that events of fault activity coincided with periods of hydrothermal activity, causing extensive hydrofracturing phenomena followed by massive fluid expulsion through the just opened fracture systems.

The circulation of hydrothermal fluids had the dual effect of causing the replacive dolomitization of the host rock, and the precipitation of dolomite cements in fractures, among breccia clasts and in other voids. The solubility of dolomite is controlled by several parameters, including temperature, pH, partial pressure of CO_2, and concentration of carbonate and other ions in the fluid. In hydrothermal systems, however, the decrease of the fluid pressure is the process most commonly invoked to explain fluid supersaturation and dolomite precipitation (e.g. Davies and Smith, 2006; Swennen *et al*., 2012). According to the above-cited fault–valve model, the abrupt release of overpressured fluids and their expulsion through fracture systems result in a significant pressure decrease. This caused a reduction of the partial pressure of CO_2 and thus an increase of the fluid saturation with respect to dolomite.

Different features, including dissolution cavities, type-4 breccias, and rounded breccia clasts, indicate that the hydrothermal system was also punctuated by limestone dissolution episodes. Calcite dissolution in hydrothermal systems is commonly attributed to a decrease of fluid temperature, because calcite solubility increases as temperature decreases (hydrothermal karst effect; Giles and de Boer, 1990). Rounded dolostone breccia clasts are the unique feature pointing to large-scale dissolution of dolomite (cf. Sharp *et al*., 2010). Nonetheless this is not conclusive evidence, as dissolution could also have affected the clasts before their dolomitization, when they were still composed of limestone. Good evidence of dolomite dissolution indeed exists albeit at a much smaller scale. The jagged outline of Dol3 saddle dolomite crystals, rimming cavities (Fig. 13B), points to the flow of aggressive fluids that resulted in the corrosion of the exposed dolomite cement crystals.

REGIONAL CONTEXT

In the classical Alpine literature, the Dauphinois–Provençal Domain has always been considered the proximal portion of the European continental margin (e.g. Debelmas and Lemoine, 1970; Debelmas and Kerckhove, 1980; Stämpfli and Marthaler, 1990), separated during the Late Triassic–Early Jurassic rifting phase of the Western Alpine Tethys, which finally led to the opening of the Ligurian–Piemonte ocean in the Bajocian (Bill *et al*., 2001). The recognition of an Early Cretaceous hydrothermal dolomitization in the Provençal Domain provides a robust, although indirect, evidence of Early Cretaceous, post-rift tectonics in this sector of the European palaeomargin. As discussed above, the inferred temperature of the hydrothermal fluids and the large volumes of the rock bodies affected by dolomitization point to a huge and very deep hydrothermal system, in turn related to deep-rooted faults which could correspond to a segment of the proto-Periadriatic transform system (sensu Handy *et al*., 2010; Fig. 22). This important E–W-trending transform fault was active since the Bajocian, accommodating differential spreading of the Piemonte and Ligurian oceans. It continued its activity in the Middle–Late Jurassic and in the Early Cretaceous, when it was possibly connected to the Iberia–Europe plate boundary, which acted as a lithosphere-scale, left-lateral strike-slip fault. This strike-slip activity continued at least until the Aptian–Albian, when a regional plate kinematic reorganization caused the divergence between Europe and Iberia and the onset of oceanic spreading in the Bay of Biscay (Tugend *et al*., 2015, and reference therein).

Extensional to strike-slip tectonics was active at least until the Aptian, and is documented both in the External Briançonnais Domain (Bertok *et al*., 2012) and in the present French subalpine domain, where it controlled the evolution of the boundary between the Provençal platform and the Dauphinois basin (e.g. Dardeau and de Graciansky, 1987; de Graciansky and Lemoine, 1988; Hibsch *et al*., 1992; Montenat *et al*., 1997, 2004; Friès and Parize, 2003; Masse *et al*., 2009).

CONCLUSIONS

Detailed field, petrographic, and geochemical analysis, as well as fluid inclusion microthermometry, allowed a comprehensive characterization of the hydrothermal dolomitization largely affecting the Mesozoic Provençal carbonates in the French-Italian Maritime Alps. The main features of this process can be summarized as follows:

- Dolomitization was a polyphase process, strictly associated with hydrofracturing events. Hydraulic fracturing was a consequence of the abrupt expulsion of overpressured fluids along main fluid-flow pathways, likely represented by high-angle faults and the related fracture systems. Circulation of hydrothermal fluids caused both replacive dolomitization of the host rock and dolomite cementation of fractures, breccias, and voids.

- Dolomitizing fluids were hot (170–260 °C), highly saline, and ^{18}O-enriched brines, likely derived from modification of seawater due to rock–fluid interactions with sedimentary as well as crystalline basement rocks during hydrothermal circulation.

– Dolomitization occurred in the earliest Cretaceous, when the Provençal carbonates were at a very shallow burial depth (from a few tens of metres to about 500 m). Therefore, the high temperature of the fluids documents a very deep hydrothermal circulation related to deep-rooted fault systems which represented the local physical expression of major changes in the tectonic regime of the Western Alpine Tethys.

The study case represents a striking example of fossil hydrothermal system where high-temperature, deep-circulating fluids lead to the dolomitization of huge volumes of carbonate rocks at unusually shallow burial depth (< 500 m). The recognition of such evidence in an Alpine setting is particularly significant since it provides a good, although indirect, evidence of pre-orogenic tectonic activity in areas where successive collisional tectonics mostly overprinted the ancient faults.

ACKNOWLEDGEMENTS

The authors thank the Associate Editor Cathy Hollis, the reviewers Alessandro Iannace and Mikel A. López-Horgue, and an anonymous reviewer, whose useful suggestions and constructive criticisms really improved the manuscript. Stefano Bernasconi and Maria Isabel Millán (ETH Geological Institute, Zurich) are kindly acknowledged for realization of C and O isotope analyses, and Simona Ferrando (Dipartimento di Scienze della Terra, Università di Torino) for guidance and assistance in fluid inclusion microthermometry. The research was supported by the University of Torino (ex 60% funds; Doctoral School of Sciences and Innovative Technologies funds) and by the Italian CNR (National Research Council), Istituto di Geoscienze e Georisorse, unità di Torino. Funds related to the ProGeoPiemonte Project (financed by Compagnia di San Paolo and University of Torino) have also been utilized. A financial contribution by the Italian Association for Sedimentary Geology (GeoSed) (Contributo Giovani 2011 to L. Barale) is gratefully acknowledged.

REFERENCES

Aranburu, A., Fernández-Mendiola, P.A., López-Horgue, M.A. and **García-Mondéjar, J.** (2002) Syntectonic hydrothermal calcite in a faulted carbonate platform margin (Albian of Jorrios, northern Spain). Sedimentology, **49**, 875–890.

Bakker, R.J. and **Baumgartner, M.** (2012) Unexpected phase assemblages in inclusions with ternary H2O–salt fluids at low temperatures. Centr. Eur. J. Geosci., **4**, 225–237.

Barale, L. (2014) The Meso–Cenozoic stratigraphic successions adjoining the Argentera Massif: stratigraphic, sedimentologic and diagenetic evidence of syndepositional tectonics. Unpubl. PhD Thesis, Università di Torino, 240 pp.

Barale, L., Bertok, C., d'Atri, A., Domini, G., Martire, L. and **Piana, F.** (2013a) Hydrothermal dolomitization of the carbonate Jurassic succession in the Provençal and Subbriançonnais Domains (Maritime Alps, North-Western Italy). Comptes-Rendus Geoscience, **345**, 47–53.

Barale, L., d'Atri, A. and **Martire, L.** (2013b) The role of microbial activity in the generation of Lower Cretaceous mixed Fe-oxide–phosphate ooids from the Provençal Domain, French Maritime Alps. J. Sed. Res., **83**, 196–206.

Barale, L., Bertok, C., d'Atri, A., Martire, L., Piana, F. and **Domini, G.** (2016) Geology of the Entracque–Colle di Tenda area (Maritime Alps, NW Italy). Journal of Maps, **12**, 359–370. DOI: 10.1080/17445647.2015.1024293

Bersezio, R. and **d'Atri, A.** (1986) Nota preliminare sulla stratigrafia del Trias medio della copertura sedimentaria del massiccio dell'Argentera nell'alta Valle Roja. Atti Acc. Naz. Lincei, **80**, 135–144.

Bertok, C., Martire, L., Perotti, E., d'Atri, A. and **Piana, F.** (2012) Kilometre-scale palaeoescarpments as evidence for Cretaceous synsedimentary tectonics in the External Briançonnais domain (Ligurian Alps, Italy). Sediment. Geol., **251**, 58–75.

Bigot, M., Damiani, L., Dellery, B. and **Durozoy, G.** (1967) Notice explicative, Carte Géologique de la France à 1:50.000, feuille Saint-Martin-Vésubie–Le Boréon. BRGM, Orléans, 29 pp.

Bill, M., O'Dogherty, L., Guex, J., Baumgartner, P. O. and **Masson, H.** (2001). Radiolarite ages in Alpine-Mediterranean ophiolites: Constraints on the oceanic spreading and the Tethys–Atlantic connection. GSA Bull., **113**, 129–143.

Boni, M., Parente, G., Bechstädt, T., De Vivo, **B.** and **Iannace, A.** (2000) Hydrothermal dolomites in SW Sardinia (Italy): evidence for a widespread late-Variscan fluid flow event. Sediment. Geol., **131**, 181–200.

Breitenbach, S.F.M. and **Bernasconi, S.M.** (2011) Carbon and oxygen isotope analysis of small carbonate samples (20 to 100 µg) with a GasBench II preparation device. Rapid Commun. Mass Spectrom., **25**, 1910-1914.

Bullen, S.R. and **Sibley ,D.F.** (1984) Dolomite selectivity and mimic replacement. Geology, 12, 655–658.

Campanino Sturani, F. (1967) Sur quelques Nérinées du Malm des Alpes Maritimes (couverture sédimentaire de l'Argentera et écailles charriées du Col de Tende). Rendiconti Acc. Naz. Lincei, **42**, 527–529.

Campredon, R. (1977) Les Formations Paléogènes des Alpes-Maritimes franco–italiennes. Mém. H.S. Soc. Géol. France, **9**, 1–199.

Carmichael, S.K. and **Ferry, J.M.** (2008) Formation of replacement dolomite in the Latemar carbonate buildup, Dolomites, Northern Italy: part2. Origin of the dolomitizing fluid and the amount and duration of fluid flow. Am. J. Sci., **308**, 885–904.

Carmichael, S.K., Ferry, J.M., and **McDonough, W.F.** (2008) Formation of replacement dolomite in the Latemar carbonate buildup, Dolomites, Northern Italy: part1. Field relations, mineralogy and geochemistry. Am. J. Sci., **308**, 851–884.

Carraro, F., Dal Piaz, G.V., Franceschetti, B., Malaroda, R., Sturani, C. and **Zanella, E.** (1970) Note Illustrative della Carta Geologica del Massiccio dell'Argentera alla scala 1: 50.000. Mem. Soc.Geol. Ital., **9**, 557–663.

Cavinato, G.P., Di Luzio, E., Moscatelli, M., Vallone, R., Averardi, M., Valente, A. and **Papale, S.** (2006) The new Col di Tenda tunnel between Italy and France: Integrated geological investigations and geophysical prospections for preliminary studies on the Italian side. Engin. Geol., **88**, 90–109.

Clayton, R.N., Friedman, I., Graf, D.L., Mayeda, T.K., Meents, W.F. and **Shimp, N.F.** (1966) The origin of saline formation waters: I. Isotopic composition. J. Geophys. Res., **71**, 3869–3882.

Costamagna, L. (2013) Middle Triassic carbonate lithostratigraphy of the Southern Briançonnais (Cottian Alps, Italy) and comparison with the surrounding areas. GeoActa, **12**, 1–24.

Dardeau, G. and **Bulard, P.F.** (1978) Répartition des dolomies du Jurassique supérieur de l’Arc de Nice (Alpes-Maritimes). Bull. B.R.G.M., **2**, 79–88.

Dardeau, G. and **de Graciansky, P.C.** (1987) Indices d’une tectonique synsédimentaire d’âge crétacé inférieur dans la basse vallée de l’Esteron (Alpes-Maritimes) et conséquences géodynamiques. Bull. Soc. Géol. Fr., 3, 1207–1210.

d’Atri, A., Piana, F., Barale, L., Bertok, C. and **Martire, L.** (2016) Geological setting of the southern termination of Western Alps. Int. J. Earth Sci., DOI: 10.1007/s00531-015-1277-91

Davies, G.R. and **Smith, L.B. Jr.** (2006) Structurally controlled hydrothermal dolomite reservoir facies: An overview. AAPG Bull., **90**, 1641–1690.

Debelmas, J. and **Lemoine, M.** (1970) The Western Alps: paleogeography and structure. Earth-Sci. Rev., **6**, 221–256.

Debelmas, J. and **Kerckhove, C.** (1980) Les Alpes franco-italiennes. Géol. Alp., **56**, 21–58.

Decarlis, A. and **Lualdi, A.** (2008) Stratigraphy and deposition of lower Cretaceous condensed deposits in the Maritime Alps (Nice arc, SE France). It. J. Geosci., **127**, 13–24.

de Graciansky, P.C. and **Lemoine, M.** (1988) Early Cretaceous extensional tectonics in the southwestern French Alps: a consequence of North-atlantic rifting during Tethyan spreading. Bull. Soc. Géol. Fr., 4, 733–737.

Dumont, T., Schwartz, S., Guillot, S., Simon-Labric, T., Tricart, P. and **Jourdan, S.** (2012) Structural and sedimentary records of the Oligocene revolution in the Western Alpine arc. J. Geodyn., **56–57**, 18–38.

Faure-Muret, A. (1955) Etudes géologiques sur le massif de l’Argentera–Mercantour et ses enveloppes sédimentaires. Mém. Carte Géol. France, Paris, 336 pp.

Faure-Muret, A., Fallot P. and **Lanteaume M.** (1967) Carte Géologique de la France à 1:50.000, feuille St-Martin-Vésubie–Le Boréon (947). Bureau de Recherches Géologiques et Minières, Orléans.

Ferry, J.M., Passey, B.H., Vasconcelos, C. and **Eiler, J.M.** (2011) Formation of dolomite at 40–80 °C in the Latemar carbonate buildup, Dolomites, Italy, from clumped isotope thermometry. Geology, **39**, 571–574.

Folk, R.L. (1962) Spectral subdivision of limestone types. In: *Classification of Carbonate Rocks*. (Ed. W.E. Ham), AAPG, Tulsa, 62–84.

Friès, G. and **Parize, O.** (2003) Anatomy of ancient passive margin slope systems: Aptian gravity-driven deposition on the Vocontian palaeomargin, western Alps, south-east France. Sedimentology, **50**, 1231–1270.

Geske, A., Goldstein, R.H., Mavromatis, V., Richter, D-K., Buhl, D., Kluge, T., John, C.M. and **Immenhauser, A.** (2015) The magnesium isotope (δ^{26} Mg) signatures of dolomites. Geochimica et Cosmochimica acta, **149**, 131–151.

Giles, M.R. and **De Boer, R.B.** (1990) Origin and significance of redistributional secondary porosity. Mar. Petrol. Geol., **7**, 379–397.

Goldberg, J.M. and **Leyreloup, A.F.** (1990) High temperature–low pressure Cretaceous metamorphism related to crustal thinning (eastern North-Pyrenean zone, France). Contrib. Mineral. Petr., **104**, 194–207.

Goldstein, R.H. and **Reynolds, T.J.** (1994) Systematics of Fluid Inclusions in Diagenetic Minerals. SEPM Short Course 31, Tulsa, 199 pp.

Guo, X., He, S., Liu, K., Cao, F., Shi, H. and **Zhu, J.** (2011) Condensates in the PY30-1 structure, Panyu Uplift, Pearl River Mouth Basin, South China Sea: evidence for hydrothermal activity associated with petroleum migration and accumulation. J. Petr. Geol., **34**, 217–232.

Handy, M. R., Schmid, S. M. , Bousquet, R. , Kissling, E. and **Bernoulli, D.** (2010) Reconciling plate-tectonic reconstructions of Alpine Tethys with the geological-geophysical record of spreading and subduction in the Alps. Earth Sci. Rev., **102**, 3-4, 121–158.

Haeri-Ardakani, O., Al-Aasm, I. and **Coniglio, M.** (2013a) Fracture mineralization and fluid flow evolution: an example from Ordovician–Devonian carbonates, southwestern Ontario, Canada. Geofluids, **13**, 1–20.

Haeri-Ardakani, O., Al-Aasm, I. and **Coniglio, M.** (2013b) Petrologic and geochemical attributes of fracture-related dolomitization in Ordovician carbonates and their spatial distribution in southwestern Ontario, Canada. Mar. Petrol. Geol., **43**, 409–422.

Hendry, J.P., Gregg, J.M., Shelton, K.L., Somerville, I.D. and **Crowley, S.F.** (2015) Origin, characteristics and distribution of fault-related and fracture-related dolomitization: Insights from Mississippian carbonates, Isle of Man. Sedimentology, **62**, 717–752.

Hewett, D.F. (1928) Dolomitization and ore deposition. Econ. Geol., **23**, 821–863.

Hibsch, C., Jandel, D., Montenat, C. and **Ott d'Estevou, P.** (1992) Evénements tectoniques crétacés dans la partie méridionale du bassin subalpin (massif Ventoux–Lure et partie orientale de l'arc de Castellane, SE France). Implications géodynamiques. Bull. Soc. Géol. France, **163**, 147–158.

Hitchon, B. and **Friedman, L.** (1969) Geochemistry and origin of formation waters in the western Canadian sedimentary basin. I. Stable isotopes of hydrogen and oxygen. Geochim. Cosmochim. Ac., **33**, 1321–1349.

Hitchon, B., Bachu, S. and **Underschulz, J.R.** (1990) Regional subsurface hydrogeology, Peace River arch area, Alberta and British Columbia. Bull. Can. Petrol. Geol., **38**, 196–217.

Hoefs J. (2009) Stable Isotope Geochemistry. 6th Edition. Springer-Verlag, Berlin–Heidelberg, 285 pp.

Iannace, A., Gasparrini, M., Gabellone, T. and **Mazzoli, S.** (2012) Late dolomitization in basinal limestones of the Southern Apennines fold and thrust belt (Italy). Oil Gas Sci. Technol., **67**, 59–75.

Iriarte, E., López-Horgue, M.A., Schroeder, S. and **Caline, B.** (2012) Interplay between fracturing and hydrothermal fluid flow in the Asón Valley hydrothermal dolomites (Basque–Cantabrian Basin, Spain). In: *Advances in carbonate exploration and reservoir analysis* (Eds. J. Garland, J.E. Neilson, S.E. Laubach and K.J. Whidden), *Geol. Soc. London, Sp. Pub.*, **370**, 207–227.

Ivaldi, J.-P, Guardia, P., Barbé, J.-F., Calvino, A., Meneroud, J.-P. and **Richard, J.-C.** (1998) Mobilité crustale et diapirism actif depuis le Crétacé au col de Tende, dans les Alpes maritimes franco–italiennes. C.R. Acad. Sci. Paris, Earth Plan. Sci., **326**, 655–662.

Jones, B. and **Luth, R.W.** (2002) Dolostones from Grand Cayman, British West Indies. J. Sed. Res., **72**, 559–569.

Knauth, L.P. and **Beeunas, M.A.** (1986) Isotope geochemistry of fluid inclusions in Permian halite with implications for the isotopic history of ocean water and origin of saline formation waters. Geochim. Cosmochim. Ac., **50**, 419–433.

Land, L.S. (1985) The origin of massive dolomite. J. Geol. Educ., **33**, 112–125.

Land, L.S. and **Prezbindowski, D.R.** (1981) The origin and evolution of saline formation waters, Lower Cretaceous carbonates, south–central Texas and southern New Mexico. J. Hydrogeol., **54**, 51–74.

Lanteaume, M. (1968) Contribution à l'étude géologique des Alpes Maritimes franco–italiennes. Mém. Carte Géol. France, Paris, 405 pp.

Lanteaume M. (1990) Carte Géologique de la France à 1:50.000, feuille Vieve–Tende (948). Bureau de Recherches Géologiques et Minières, Orléans.

Lapponi, F., Bakker, R.J. and **Bechstäedt, T.** (2007) Low temperature behaviour of natural saline fluid inclusions in saddle dolomite (Paleozoic, NW Spain). Terra Nova, **19**, 440–444.

Lapponi, F., Bechstäedt, T., Boni, M., Banks, D.A. and **Schneider, J.** (2014) Hydrothermal dolomitization in a complex geodynamic setting (Lower Palaeozoic, northern Spain). Sedimentology, **61**, 411–443.

Lavoie, D., Chi, G., Brennan-Alpert, P., Desrochers, A. and **Bertrand, R.** (2005) Hydrothermal dolomitization in the Lower Ordovician Romaine Formation of the Anticosti Basin: significance for hydrocarbon exploration. Bull. Can. Petrol. Geol., **53**, 454–471.

Littler, K., Robinson, S.A., Bown, P.R., Nederbragt, A.J. and **Pancost, R.D.** (2011) High sea-surface temperatures during the Early Cretaceous Epoch. Nature, **4**, 169–172.

López-Horgue, M.A., Iriarte, E., Schröeder, S., Fernández-Mendiola, P.A., Caline, B., Corneyllie, H., Frémont, J., Sudrie, M. and **Zerti, S.** (2010) Structurally controlled hydrothermal dolomites in Albian carbonates of the Asón valley, Basque Cantabrian Basin, Northern Spain. Mar. Petrol. Geol., **27**, 1069–1092.

Machel, H.G. (2004) Concepts and models of dolomitization: a critical reappraisal. In: *The Geometry and Petrogenesis of Dolomite Hydrocarbon Reservoirs* (Eds. C.J.R. Braithwaite, G. Rizzi and G. Darke), *Geol. Soc. London, Sp. Pub.*, 235, 7–63.

Machel, H.G. and **Lonnee, J.** (2002) Hydrothermal dolomite – a product of poor definition and imagination. Sediment. Geol., **152**, 163–171.

Malaroda, R. (Ed.) (1970) Carta Geologica del Massiccio dell'Argentera alla scala 1:50.000. Mem. Soc. Geol. Ital., **9**.

Malaroda, R. (1999) L'Argentera meridionale – Memoria illustrativa della "Geological Map of Southern Argentera Massif (Maritime Alps) 1 :25 000". Mem. Sci. Geol., **51–52**, 241–331.

Masse, J.-P., Villeneuve, M., Leonforte, E.-and **Nizou, J.** (2009) Block tilting of the North Provence early Cretaceous carbonate margin: stratigraphic, sedimentologic and tectonic data. Bull. Soc. Géol. France, **180**, 105–115.

McCrea, J.M. (1950) On the isotopic chemistry of carbonates and paleotemperature scale. J. Chem. Phys., **18**, 849–857.

Montenat, C., Hibsch, C., Perrier, J.C., Pascaud, F. and **De Bretizel, P.** (1997) Tectonique cassante d'âge crétacé inférieur dans l'Arc de Nice (Alpes-Maritimes, France). Géol. Alp., **73**, 59–66.

Montenat, C., Janin, M.-C. and **Barrier, P.** (2004) L'accident du Toulourenc: une limite tectonique entre la plate-forme provençale et le Bassin vocontien à l'Aptien–Albien (SE France). C. R. Geoscience, **336**, 1301–1310.

Morrow, D.W. (1982) Descriptive field classification of sedimentary and diagenetic breccia fabrics in carbonate rocks. Bull. Can. Petrol. Geol., **30**, 227–229.

Murray, R.C. and **Lucia, F.J.** (1967) Cause and control of dolomite distribution by rock selectivity. GSA Bull., **78**, 21–35.

Nader, F.H., López-Horgue, M.A., Shah, M.M., Dewit, J., Garcia, D., Swennen, R., Iriarte, E., Muchez, P. and **Caline, B.** (2012) The Ranero hydrothermal dolomites (Albian, Karrantza Valley, Northwest Spain): implications on conceptual dolomite models. Oil Gas Sci. Technol., **67**, 9–29.

Nunn, E.V. and **Price, G.D.** (2010) Late Jurassic (Kimmeridgian–Tithonian) stable isotopes ($\delta^{18}O$, $\delta^{13}C$) and Mg/Ca ratios: New palaeoclimate data from Helmsdale, northeast Scotland. Palaeogeogr. Palaeocl., **292**, 325–335.

Ohle, E.L. (1985) Breccias in Mississippi valley-type deposits. Econ. Geol., **80**, 1736–1752.

Phillips, W.J. (1972) Hydraulic fracturing and mineralization. J. Geol. Soc. London, 128, 337–359.

Piana, F., Musso, A., Bertok, C., d'Atri, A., Martire, L., Perotti, E., Varrone, D. and **Martinotti, G.** (2009) New data on post-Eocene tectonic evolution of the External Ligurian Briançonnais (Western Ligurian Alps). It. J. Geosci., **128**, 353–366.

Podlaha, O.G., Mutterlose, J. and **Veizer, J.** (1998) Preservation of $\delta^{18}O$ and $\delta^{13}C$ in belemnite rostra from the Jurassic/Early Cretaceous successions. Am. J. Sci., **298**, 324–347.

Pouchou, J.L. and **Pichoir, F.** (1988) Determination of mass absorption coefficients for soft X-rays by use of the electron microprobe. In: *Microbeam Analysis* (Ed. Newbury D.E.), pp. 319–324. San Francisco Press, San Francisco.

Ramsay, J.G. (1980) The crack-seal mechanism of rock deformation. Nature, **284**, 135–139.

Richter, D.K., Neuser, R.D., Schreuer, J., Gies, H. and **Immenhauser, A.**, (2011) Radiaxial-fibrous calcites: a new look at an old problem. Sed. Geol., **239**, 23–36.

Ronchi, P., Jadoul, F., Ceriani, A., Di Giulio, A., Scotti, P., Ortenzi, A. and **Previde Massara, E.** (2011) Multistage dolomitization and distribution of dolomitized bodies in Early Jurassic carbonate platforms (Southern Alps, Italy). Sedimentology, **58**, 532–565.

Ronchi, P., Masetti, D., Tassan, S. and **Camocino, D.** (2012) Hydrothermal dolomitization in platform and basin carbonate successions during thrusting: A hydrocarbon reservoir analogue (Mesozoic of Venetian Southern Alps, Italy). Mar. Petrol. Geol., **29**, 68–89.

Rosenbaum, J. and **Sheppard ,S.M.** (1986) An isotopic study of siderites, dolomites and ankerites at high temperatures, Geochim. Cosmochim. Acta **50**, 1147-1150.

Rouire, J., Autran, A., Prost, A., Rossi, P. and **Rousset, C.** (1980) Carte Géologique de la France à 1:250.000, feuille Nice (40). Bureau de Recherches Géologiques et Minières, Orléans.

Schouten, S., Hopmans, E.C., Forster, A., Van Breugel, Y., Kuypers, M.M. and **Sinninghe Damsté, J.S.** (2003) Extremely high sea-surface temperatures at low latitudes during the middle Cretaceous as revealed by archaeal membrane lipids. Geology, **31**, 1069–1072.

Shah, M.M., Nader, F.H., Garcia, D., Swennen, R. and **Ellam, R.** (2012) Hydrothermal dolomites in the Early Albian (Cretaceous) platform carbonates (NW Spain): nature and origin of dolomites and dolomitizing fluids. Oil Gas Sci. Technol., **67**, 97–122.

Sharp, I., Gillespie, P., Morsalnezhad, D., Taberner, C., Karpuz, R., VergéS, J., Horbury, A., Pickard, N., Garland, J. and **Hunt, D.** (2010) Stratigraphic architecture and fracture-controlled dolomitization of the Cretaceous Khami and Bangestan groups: an outcrop case study, Zagros Mountains, Iran. In: *Mesozoic and Cenozoic carbonate systems of the Mediterranean and the Middle East: stratigraphic and diagenetic reference models.* (Eds. F. S. P.Van Buchem, K. Gerdes and M. Esteban), *Geol. Soc. London, Sp. Pub.*, 329, 343–396.

Shepherd, T. J., Rankin, A. H. and **Alderton, D.H.M.** (1985) A practical guide to fluid inclusion studies. Blackie Publishing Co., London, 239 pp.

Sibley, D.F. (1982) The origin of common dolomite fabrics: clues from the Pliocene. J. Sed. Petrol., **52**, 1087–1100.

Sibley, D.F. and **Gregg, J.M.** (1987) Classification of dolomite rock textures. J. Sed. Petrol., **57**, 967–975.

Sibson, R.H. (1987) Earthquake rupturing as a mineralizing agent in hydrothermal systems. Geology, **15**, 701–704.

Sibson, R.H. (1992) Implications of fault–valve behaviour for rupture nucleation and recurrence. Tectonophysics, **211**, 283–293.

Sinclair, H.D. (1997) Tectonostratigraphic model for underfilled peripheral foreland basins: an Alpine perspective. GSA Bull., **109**, 324–346.

Spencer-Cervato, C. and **Mullis, J.** (1992) Chemical study of tectonically controlled hydrothermal dolomitization: an example from the Lessini Mountains, Italy. Geol. Rundsch., **81**, 347–370.

Stämpfli, G.M. and **Marthaler, M.** (1990) Divergent and convergent margins in the north-western Alps – Confrontation and actualistic models. Geodin. Acta, **4**, 159–184.

Swennen, R., Dewit, J., Fierens, E., Muchez, P., Shah, M., Nader, F. and **Hunt, D.** (2012) Multiple dolomitization events along the Pozalagua Fault (Pozalagua Quarry, Basque–Cantabrian Basin, Northern Spain). Sedimentology, **59**, 1345–1374.

Tugend, J., Manatschal, G. and **Kusznir, N.J.** (2015) Spatial and temporal evolution of hyperextended rift systems: Implication for the nature, kinematics, and timing of the Iberian-European plate boundary. Geology, **43**, 1, 15–18.

Vacherat, A., Mouthereau, F., Pik, R., Bernet, M., Gautheron, C., Masini, E., Le Pourhiet, L., Tibari, B. and **Lahfid, A.** (2014) Thermal imprint of rift-related processes in orogens as recorded in the Pyrenees. Earth Planet. Sci. Lett., **408**, 296–306.

FIGURE CAPTIONS

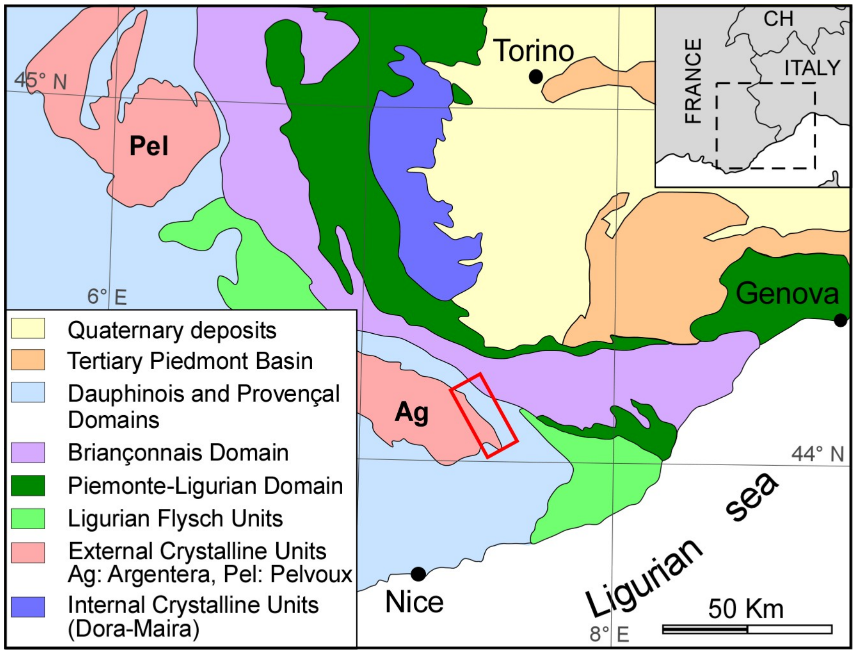

Fig. 1. Schematic Geographical and geological map of the SW Alps. The red rectangle indicates the location of the study area and corresponds to Fig. 2.

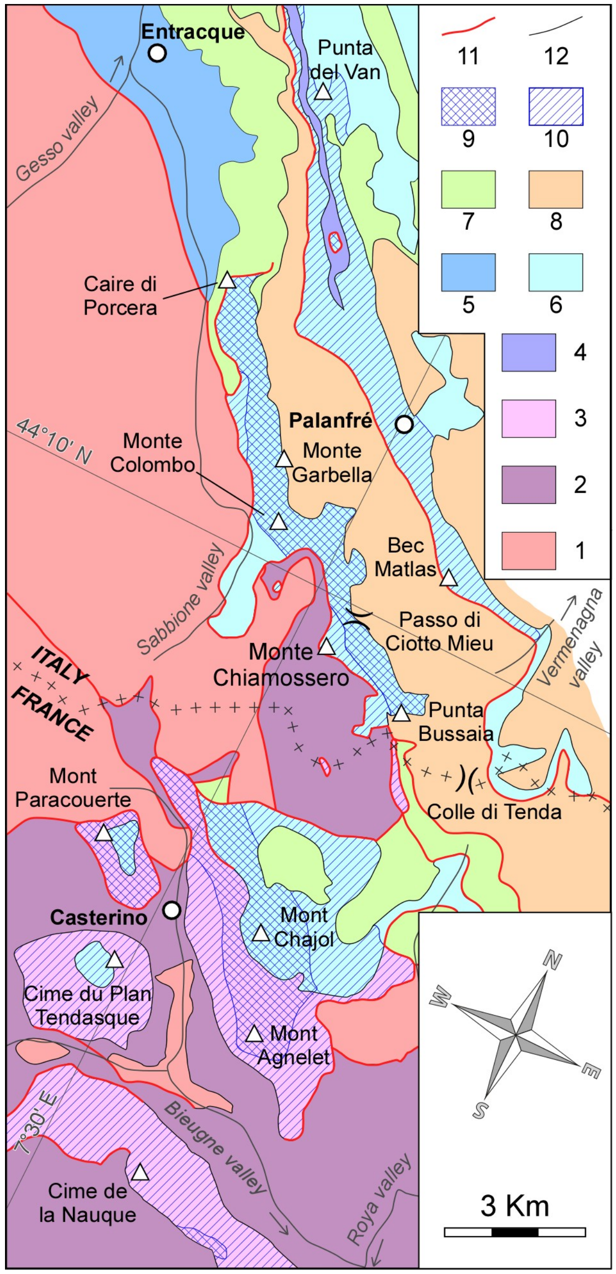

Fig. 2. Geological scheme of the study area, showing the dolomitization degree of Middle Triassic–Jurassic carbonates (the location of the study area is also reported in the geological scheme of Fig. 5). 1: Argentera Massif crystalline basement. 2: Permian–Lower Triassic siliciclastic deposits. 3: Middle Triassic carbonates. 4: Upper Triassic–Lower Jurassic succession. 5: Jurassic Dauphinois hemipelagic succession. 6: Middle Jurassic–Berriasian Provençal carbonates (Garbella Limestone). 7: Cretaceous succession. 8: Alpine Foreland Basin succession. 9: intense hydrothermal dolomitization (local complete dolomitization of the host rock; common dolomite vein frameworks and dolomite-cemented breccias). 10: moderate

hydrothermal dolomitization (partial dolomitization of the host rock; rare dolomite vein networks and dolomite-cemented breccias). 11: main faults. 12: stratigraphic contacts. Modified from: Barale *et al*., (2016) (Italian part); Faure-Muret *et al*., (1967), and Lanteaume, (1990) (French part).

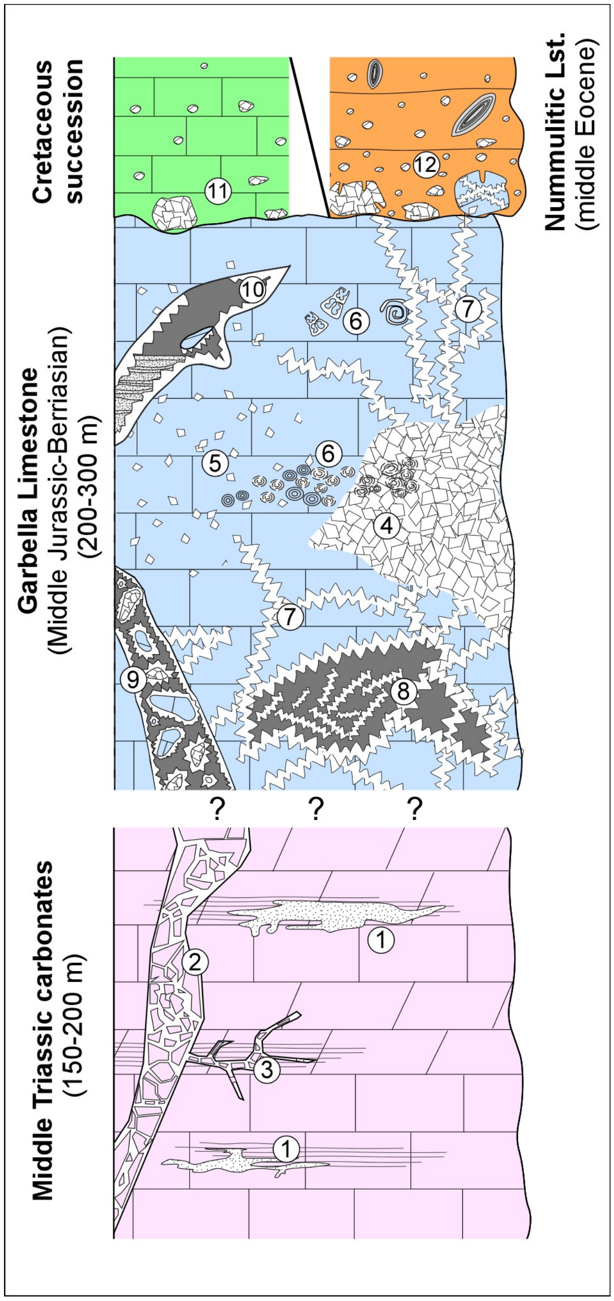

Fig. 3. Schematic stratigraphic log of the Middle Triassic–Paleogene succession in the study area, showing the vertical distribution of the main dolomitization facies, breccia types, cavities, and the occurrence of reworked dolomite. 1: decimetre-sized, stratabound, completely

dolomitized bodies. 2: subvertical bodies of type-1 breccias. 3: minor, bed-parallel type-1 breccia bodies. 4: metre- to decametre-sized, completely dolomitized bodies. 5: non-selective partial dolomitization. 6: grain-selective partial dolomitization. 7: veined limestones. 8: boxwork fabrics and dolomite-vein breccias (type-4). 9: type-2 breccias. 10: dolomite-cemented dissolution cavities. 11: reworked dolomite in the Cretaceous succession. 12: reworked dolomite in the lowermost interval of middle Eocene Nummulitic Limestone.

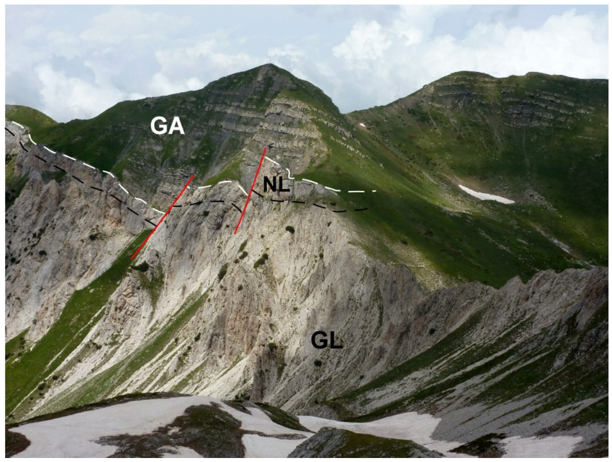

Fig. 4. Panoramic view of the western side of Passo di Ciotto Mieu. Dolomitized Garbella Limestone (GL) are unconformably overlain by the Alpine Foreland Basin succession (Nummulitic Limestone and *Globigerina* Marl, NL; Grès d'Annot, GA). The whitish colour of the Garbella Limestone reflects a high degree of dolomitization. The cliff of Garbella Limestone in the centre of the image is about 100 metres high; image taken from Monte Chiamossero eastern side (44°09'29.0"N, 7°30'44.8"E), looking north.

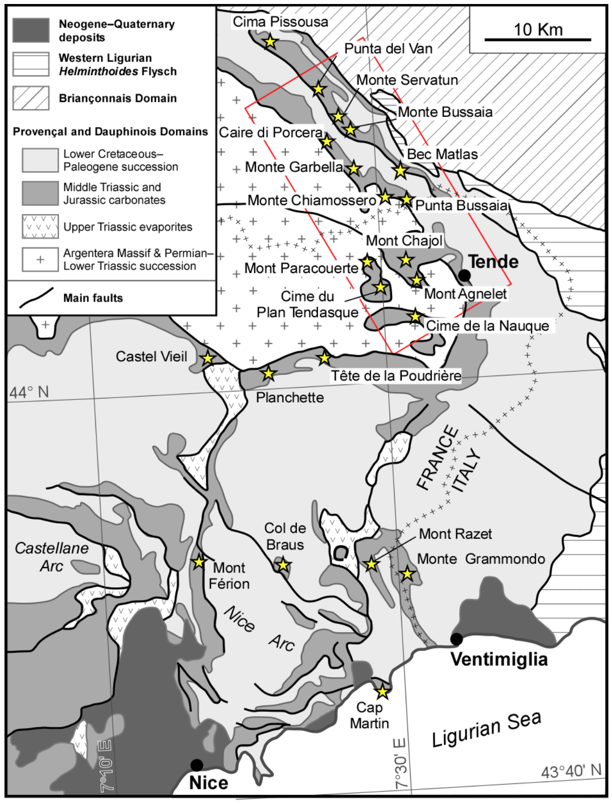

Fig. 5. Geological scheme of the French–Italian southern Maritime Alps (redrawn from Rouire *et al.*, 1980), showing the distribution of the hydrothermal dolomite outcrops (stars). The red rectangle indicates the location of the study area and corresponds to Fig. 2.

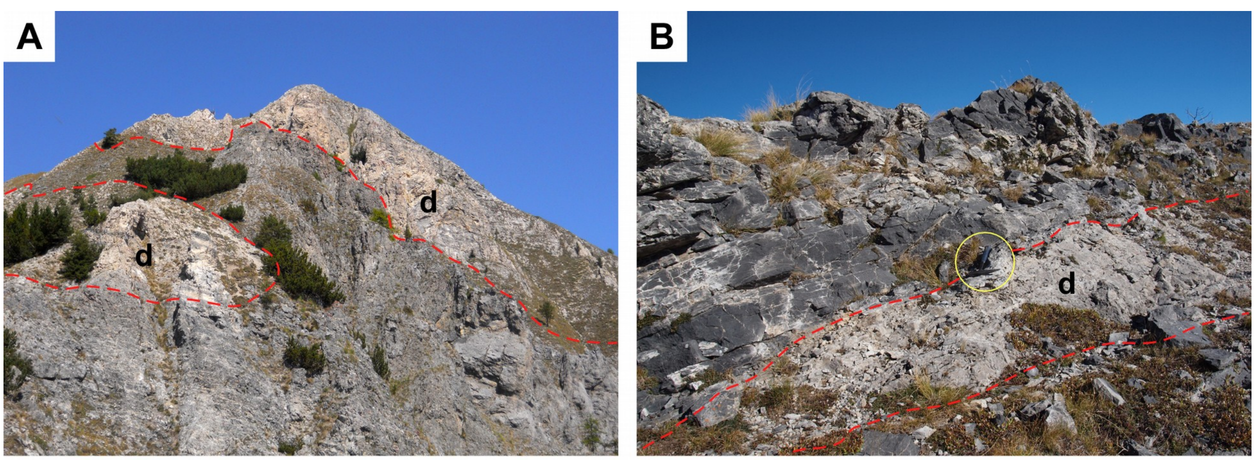

Fig. 6. Field features of dolomitized rock bodies. (A) Discontinuous, decametre-thick, white-coloured, pervasively dolomitized rock bodies (d) within the grey-coloured, partially dolomitized Upper Triassic–Jurassic carbonates on Mont Chajol southern side. The image shows a portion of cliff about 110 metres high, and has been taken from Mont Chajol southern ridge

(44°05'58.4"N, 7°31'50.6"E), looking north. (B) Stratabound, decimetre-thick, completely dolomitized rock body (d) in the Middle Triassic carbonates of Mont Agnelet (44°05'14.3"N, 7°31'56.5"E); encircled hammer for scale.

Fig. 7. Complex network of decimetre-thick, tabular bodies of dolomite-cemented breccia in evenly bedded Middle Triassic carbonates (Mont Paracouerte southern side; 44°06'14.5"N, 7°29'05.9"E); breccia bodies either crosscut at a high angle the host-rock bedding or develop parallel to it.

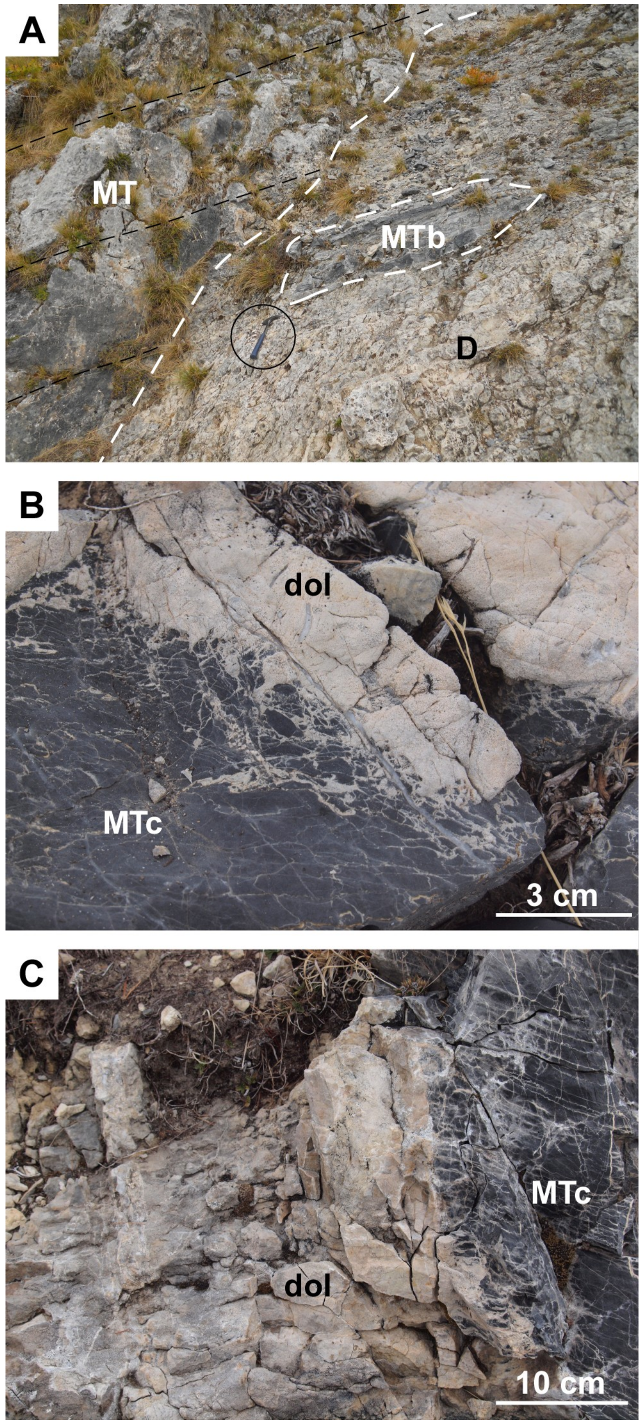

Fig. 8. (A) Subvertical body made up of coarsely to very coarsely crystalline dolostones and dolomite-cemented breccias (D), showing a sharp contact with the poorly dolomitized Middle Triassic host rock (MT) and embedding a metre-sized, angular block of the same Middle Triassic carbonates (MTb); Mont Agnelet (44°05'16.5"N, 7°31'53.0"E). Black lines indicate the bedding of Middle Triassic carbonates (encircled hammer for scale). (B) Stratabound,

decimetre-thick, light-coloured, completely dolomitized body (dol) within Middle Triassic carbonates (MTc), showing an incipient nodular structure. At the boundary of the dolomitized body, dolomitization affects the internodular matrix but not the nodules themselves (Mont Agnelet; 44°05'13.6"N, 7°31'57.0"E). (C) Subvertical, light-coloured, completely dolomitized body (dol) within Middle Triassic carbonates (MTc), showing a sharp contact with the host rock. Mont Agnelet (44°05'14.3"N, 7°31'56.8"E).

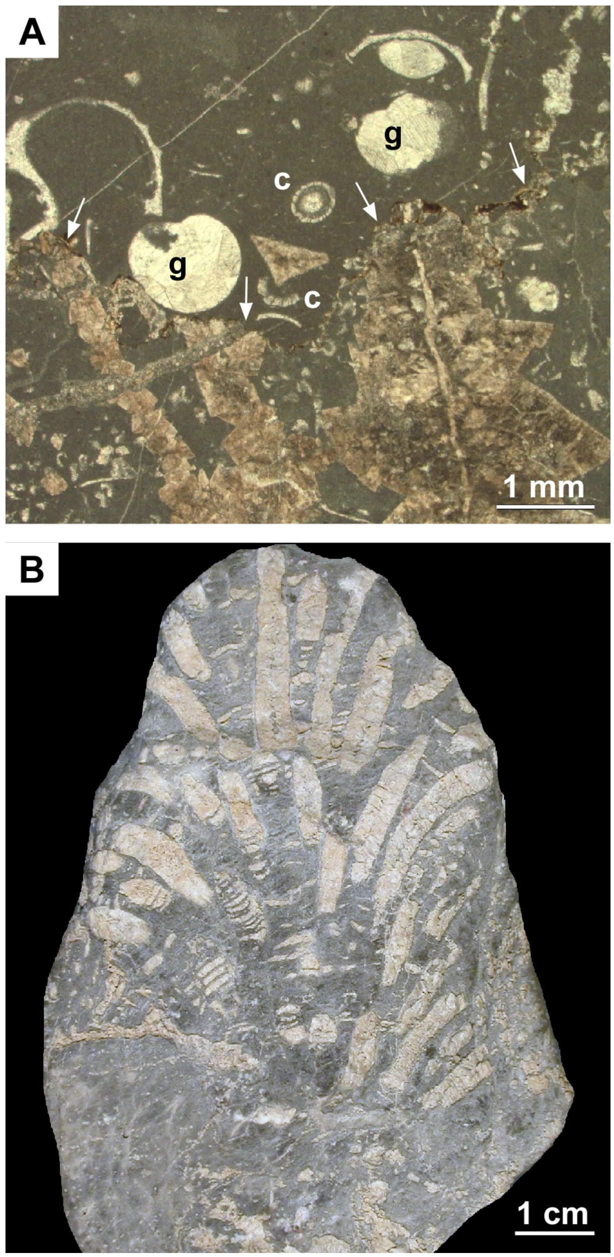

Fig. 9. (A) Transmitted-light photomicrograph showing a bedding-parallel, burial stylolite (arrows) which separates a bioclastic wackestone crossed by dolomite veins (in the lower part)

from an undolomitized bioclastic wackestone with gastropod moulds (g), charophytae gyrogonites (c), and other bioclasts (in the upper part). Note that dolomite veins are clearly cut by the stylolite. Upper part of the Garbella Limestone, Monte Colombo. (B) Selective replacement of corals in a coral boundstone (Garbella Limestone, Sabbione Valley).

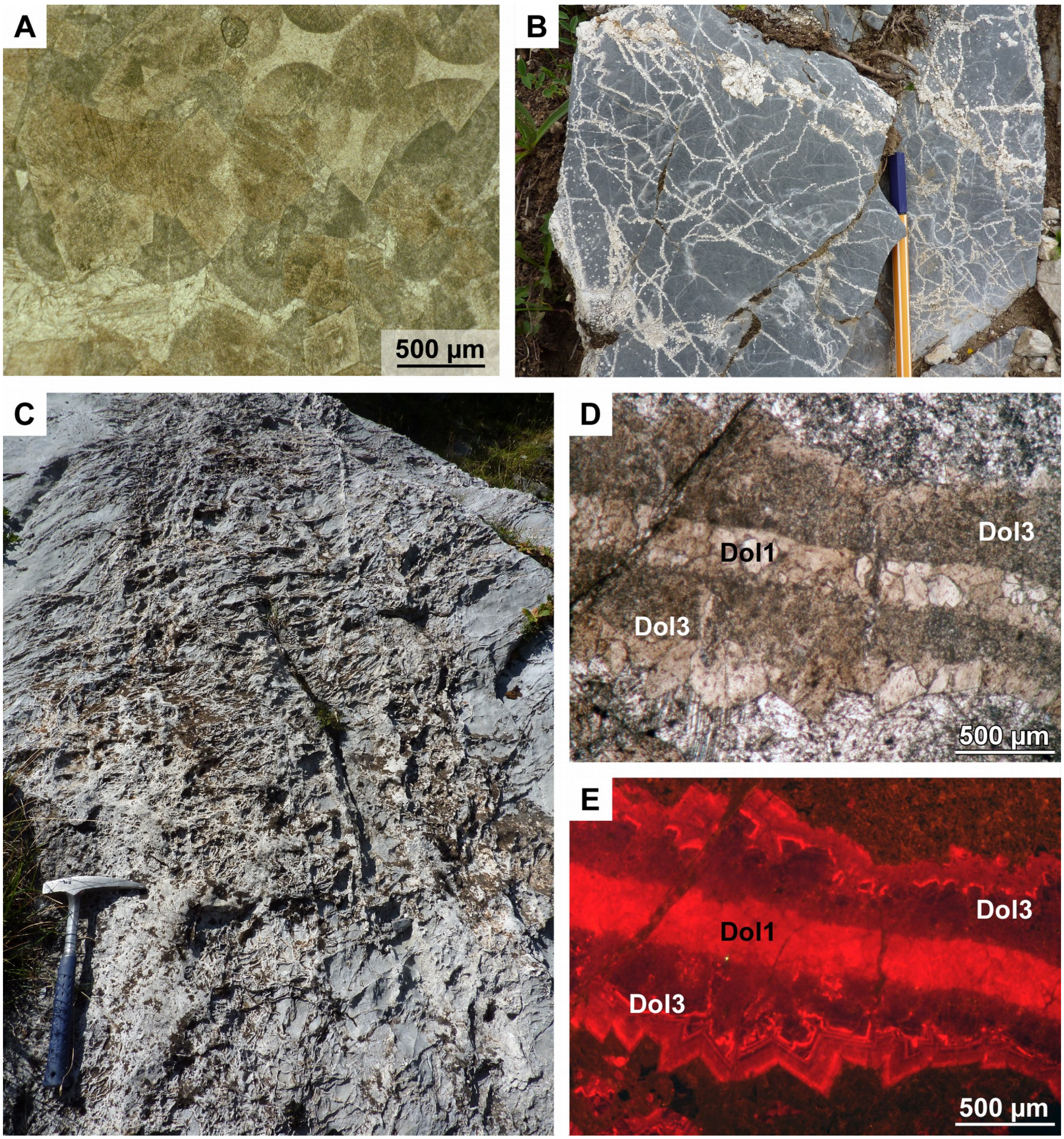

Fig. 10. Partial-dolomitization fabrics: (A) Transmitted-light photomicrograph showing a non-selective dolomitization of an ooidal grainstone: euhedral dolomite crystals grow indifferently on the ooids and on the cement. (B) Network of dolomite veins crossing the Garbella Limestone (Passo di Ciotto Mieu; 44°09'47.9"N, 7°30'46.1"E). A few isolated dolomite crystals also occur in the host rock. (C) Sub-vertical, decimetre-wide, tabular rock volume characterized by a very high density of dolomite veins, crossing the Garbella Limestone (Palanfré; 44°10'28.1"N, 7°29'44.0"E). (D), (E) Transmitted-light photomicrograph (D) and cathodoluminescence image of a dolomite vein crossing the Garbella Limestone, showing a thin inner part composed of medium crystalline, turbid dolomite (Dol1), and a thicker outer part composed of outward growing, coarse dolomite crystals (Dol3).

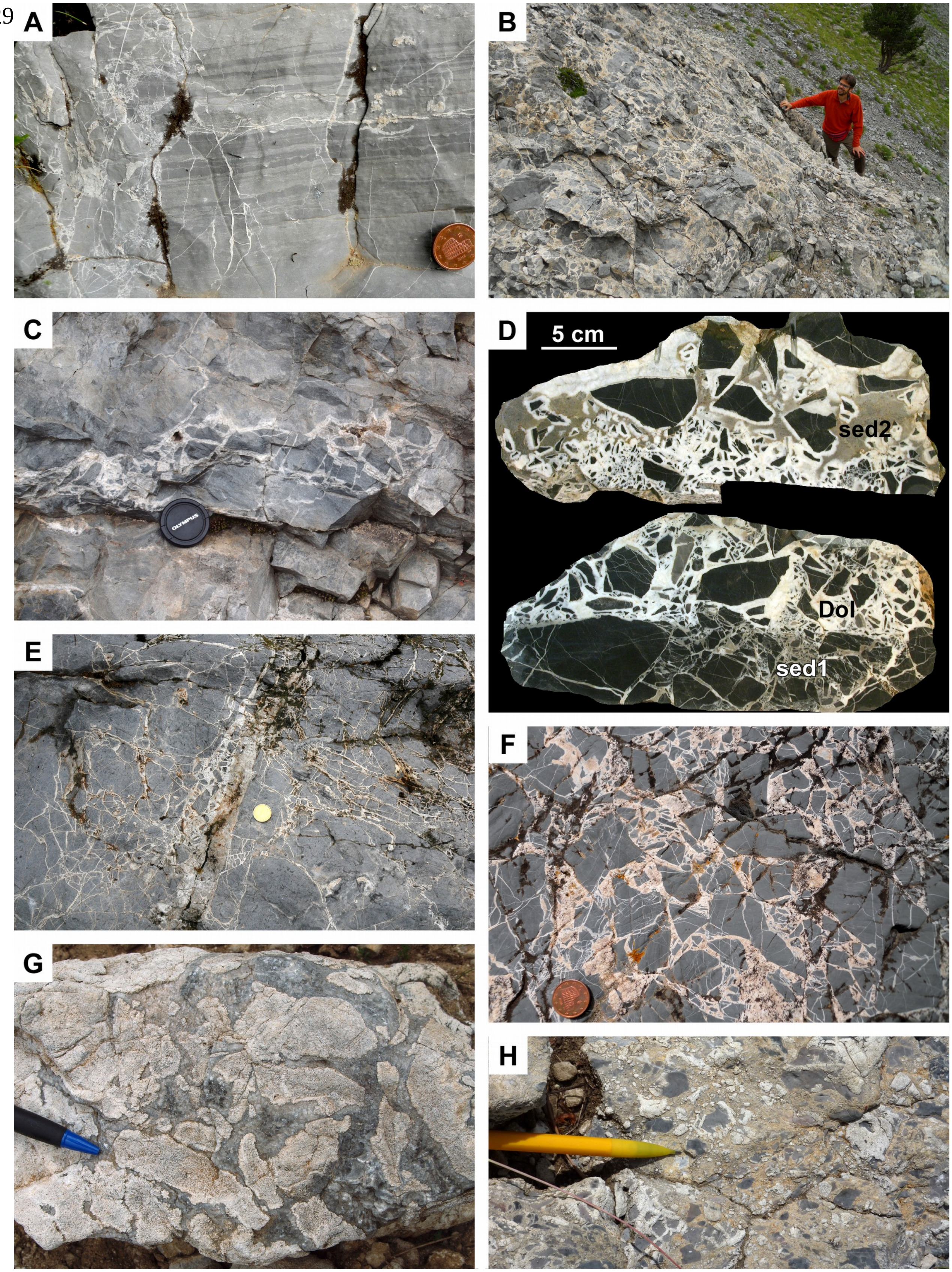
A
B
C
D
5 cm
sed2
Dol
sed1
E
F
G
H

Fig. 11. Breccia features: (A) Centimetre-large, tabular breccia body crossing the bedding of finely laminated Middle Triassic carbonates at a high angle (fallen block on Mont Paracouerte western side; 44°06'10.8"N, 7°29'03.3"E). (B) Irregularly shaped, metre-sized breccia body in Middle Triassic carbonates (Mont Paracouerte; 44°06'14.4"N, 7°29'06.9"E). (C) Type-1 breccia in Middle Triassic carbonates, made up of centimetre-sized, angular clasts showing a jigsaw-puzzle arrangement (Mont Agnelet; 44°05'12.0"N, 7°31'58.5"E). (D) Two polished hand samples (juxtaposed in their relative position) of a type-1 breccia, made up of clasts of Middle Triassic carbonates, and showing a complex void filling. In the lower part, voids between clasts are filled with a grey, micritic sediment (sed1), which is followed by a white dolomite cement (Dol), in turn followed by a micritic, brownish sediment in the upper part (sed2) (Cime du Plan Tendasque; 44°05'27.4"N, 7°29'49.0"E). (E) Tabular body of type-1 breccia crossing a veined volume of Garbella Limestone (Sabbione Valley; 44°10'13.6"N, 7°28'37.5"E). Note the gradual transition between the breccia body and the veined limestones, occurring by a progressive increase of clast displacement resulting in the formation of centimetre-wide voids filled with coarse dolomite cement. (F) Type-1 breccia composed of centimetre-sized clasts of Middle Triassic carbonates, in turn locally crossed by millimetre-thick dolomite veins (fallen block on Mont Paracouerte western side; 44°06'13.7"N, 7°28'53.6"E). (G) Type-2 breccia, consisting of centimetre-sized, subrounded clasts of coarsely crystalline dolostones. Voids between clasts are cemented by a millimetre- to centimetre-thick rim of coarsely to very coarsely crystalline, white dolomite, with dark-coloured calcite plugging the remaining pores (near Passo di Ciotto Mieu; 44°09'51.1"N 7°31'12.1"E). (H) Type-3, polymictic, clast-supported breccia with centimetre-sized, angular to subrounded, clasts, composed of dolostones, limestones and partially dolomitized limestones, in a micritic matrix containing sand-sized clasts of the same lithologies as larger clasts (Passo di Ciotto Mieu; 44°09'49.6"N, 7°30'48.2"E).

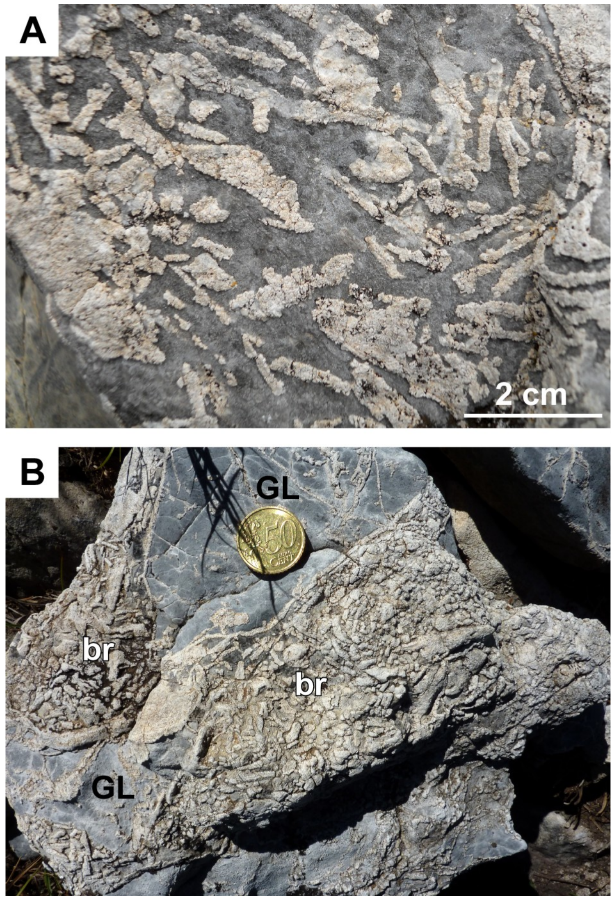

Fig. 12. Breccia features: (A) Close-up view of a type-4 breccia, mostly composed of millimetre- to centimetre-long and millimetre-wide, plate-like clasts made up of coarsely crystalline dolomite. Voids between clasts are cemented by dark-grey, sparry calcite (eastern side of Sabbione valley). (B) Centimetre-large tabular bodies of type-4 breccia (br), bordered by veins in the host Garbella Limestone (GL) (Monte Colombo).

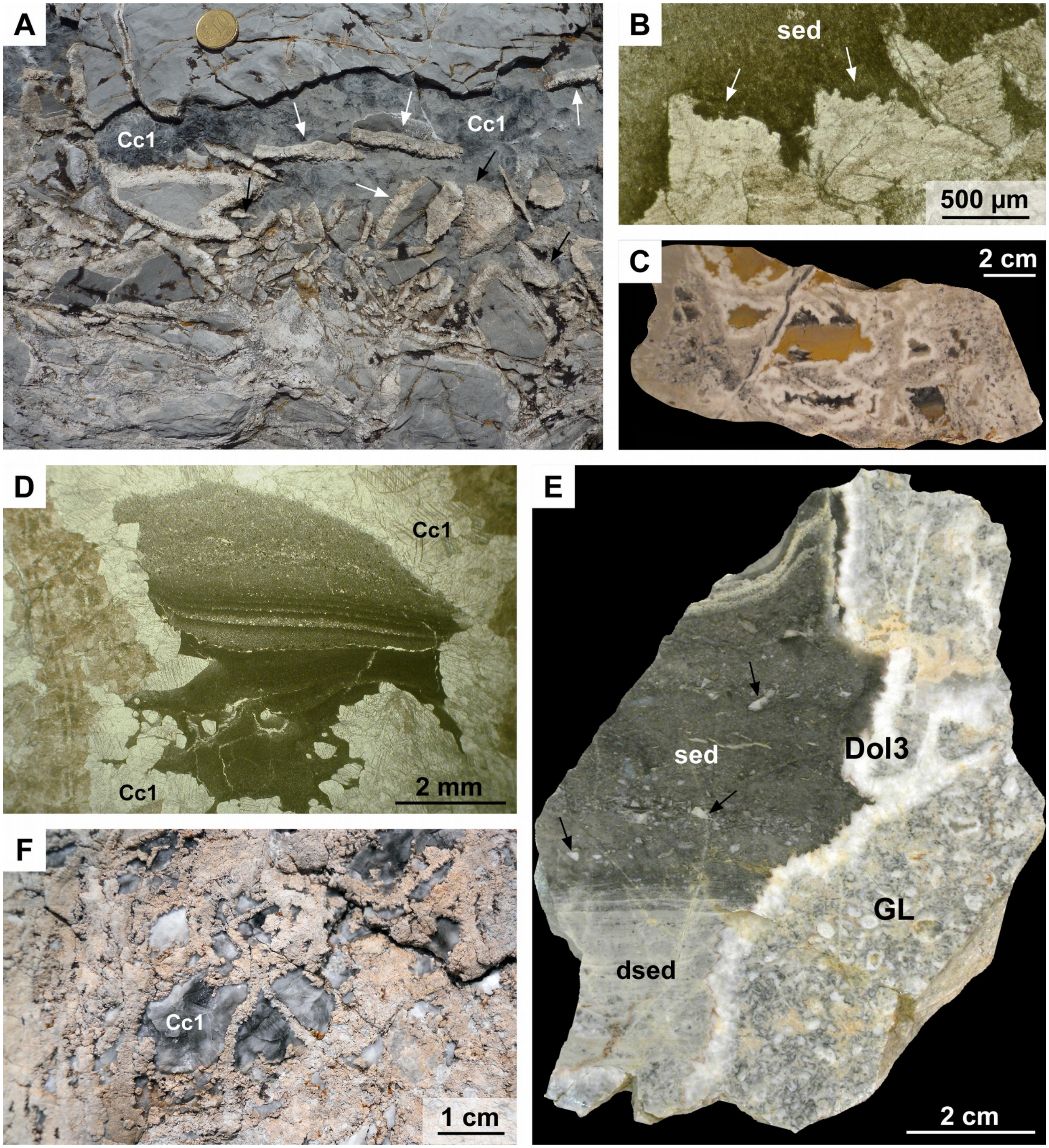

Fig. 13. Cavity features: (A) Large dissolution cavity in Middle Triassic carbonates. The occurrence of clasts with asymmetric white, very coarsely crystalline dolomite cement rims (saddle dolomite Dol 3, white arrows) and clasts entirely made up of the same dolomite cement (black arrows) indicate that cavity walls were fractured after precipitation of a coarse dolomite cement rim on them and before being plugged by a dark-coloured sparry calcite (Cc1). (Monte Chiamossero; 44°09'28.6"N, 7°30'50.5"E). (B) Transmitted-light photomicrograph showing a

portion of a dissolution cavity rimmed by a coarsely crystalline dolomite cement (saddle dolomite Dol3), and filled by a fine-grained sediment (sed). Note the jagged outline of dolomite crystals (arrows), due to dissolution of crystal faces. (C) Polished hand sample showing centimetre-sized cavities within completely dolomitized Garbella Limestone, rimmed by a white, very coarsely crystalline dolomite cement (saddle dolomite Dol3) and filled by mustard-coloured internal sediments, giving rise in some cases to geopetal structures plugged by a sparry dark-coloured calcite cement (Cc1) (eastern side of Sabbione Valley). (D) Transmitted-light photomicrograph of a centimetre-sized cavity hosting silt-sized internal sediments, locally organized into graded laminae. Cavity walls are rimmed by a sparry calcite cement (Cc1). (E) Polished hand sample showing a large dissolution cavity in partially dolomitized bioclastic–oncoidal rudstones of the Garbella Limestone (GL). The cavity is rimmed by a white, very coarsely crystalline dolomite cement (saddle dolomite Dol3) and filled by two different sediments. A first layer of laminated, dolomitized sediment (dsed) is followed by a second one of undolomitized sediment (sed), containing fragments of Dol3 crystals (arrows) (Monte Chiamossero; 44°09'36.0"N, 7°31'24.8"E). (F) Boxwork fabric in the Garbella Limestone: centimetre-sized cavities, filled with a sparry, locally dark-coloured, calcite cement (Cc1), are divided by a complex 3D network of thin dolomite veins. (Passo di Ciotto Mieu; 44°09'48.6"N, 7°30'45.4"E).

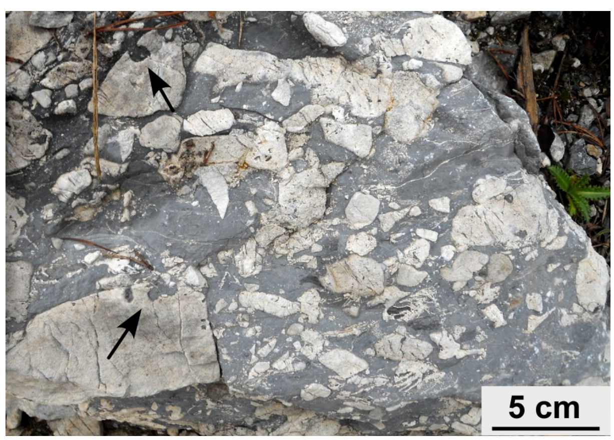

Fig. 14. Upper surface of a conglomerate bed in the basal interval of the Nummulitic Limestone, made up of clasts of dolomitized Garbella Limestone locally showing *Gastrochaenolites* bivalve borings (arrows). (Monte Garbella; 44°10'12.9"N, 7°28'39.8"E).

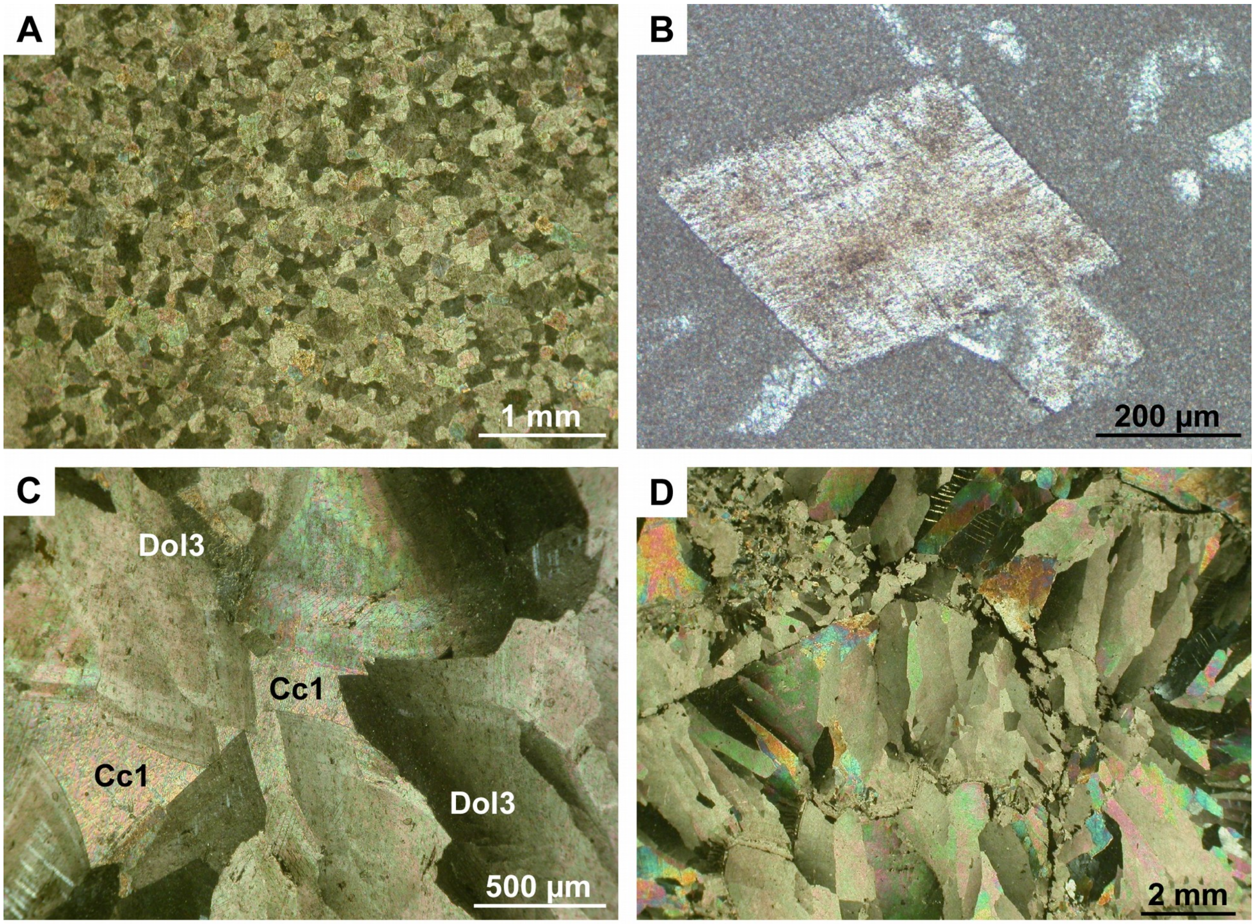

Fig. 15. (A) Transmitted-light, crossed polars photomicrograph of a Garbella Limestone sample, fully dolomitized by finely to medium crystalline, subhedral Dol1 replacement dolomite. (B) Transmitted-light photomicrograph showing a coarse, euhedral crystal of Dol2 replacement dolomite, growing in a mudstone bed of the Garbella Limestone. (C) Transmitted-light, crossed polars photomicrograph showing a detail of a cavity cemented by coarsely to very coarsely crystalline, Dol3 saddle dolomite, with Cc1 calcite plugging the remaining voids. Note: the curved crystal faces, the zoning, and the sweeping extinction of Dol3. (D) Transmitted-light, crossed polars photomicrograph showing very coarsely crystalline fascicular-optic Dol4 dolomite cements. Note the sweeping extinction of the crystals.

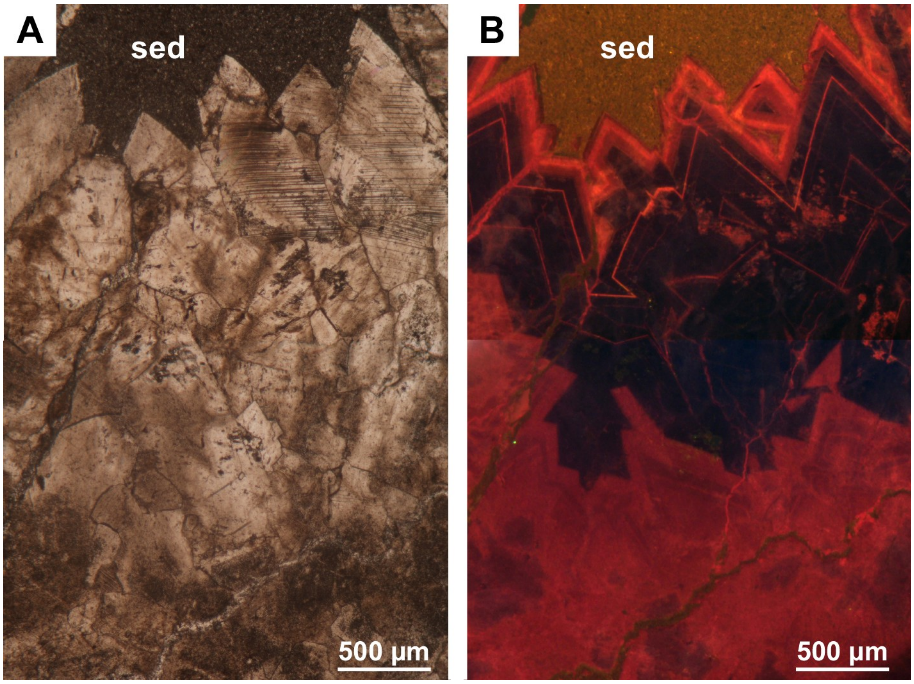

Fig. 16. Transmitted light (A) and cathodoluminescence (B) photomicrographs of a very coarsely crystalline, Dol3 saddle dolomite rimming a cavity, and overlain by a fine-grained, calcitic sediment (sed). Dol3 crystals have a thick inner part with dull to moderate red–orange luminescence, followed by a thick non-luminescent zone with hairline, moderately to brightly luminescent, orange zones, and by an outer part with moderate to bright, red–orange luminescence zones.

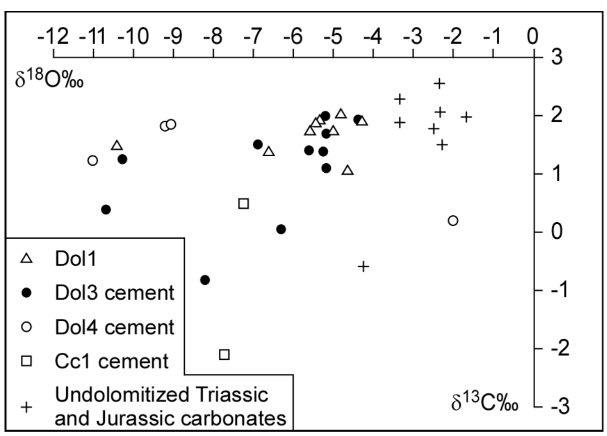

Fig. 17. Stable isotope data: $\delta^{18}O$ versus $\delta^{13}C$ cross-plot for Dol1, Dol3 and Dol4 dolomite, for Cc1 calcite, and for Triassic and Jurassic host carbonates (values relative to VPDB standard).

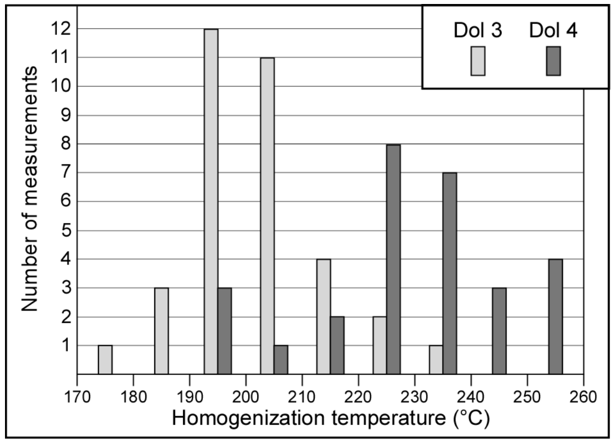

Fig. 18. Histogram of the homogenization temperatures obtained for Dol3 saddle dolomite and for Dol4 cements.

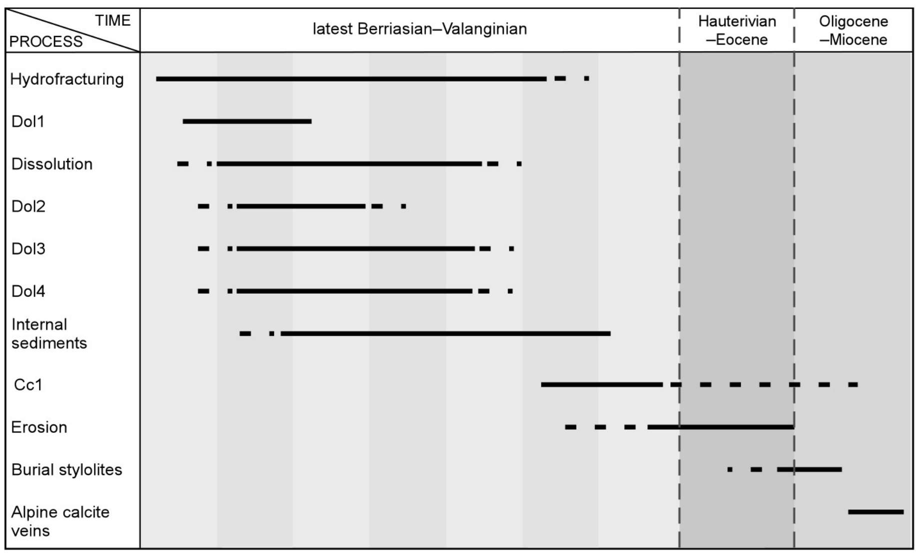

Fig. 19. Schematic paragenetic sequence showing the relative timing of the processes that affected the host rocks during and after hydrothermal dolomitization. Dashed lines indicate the uncertainty range.

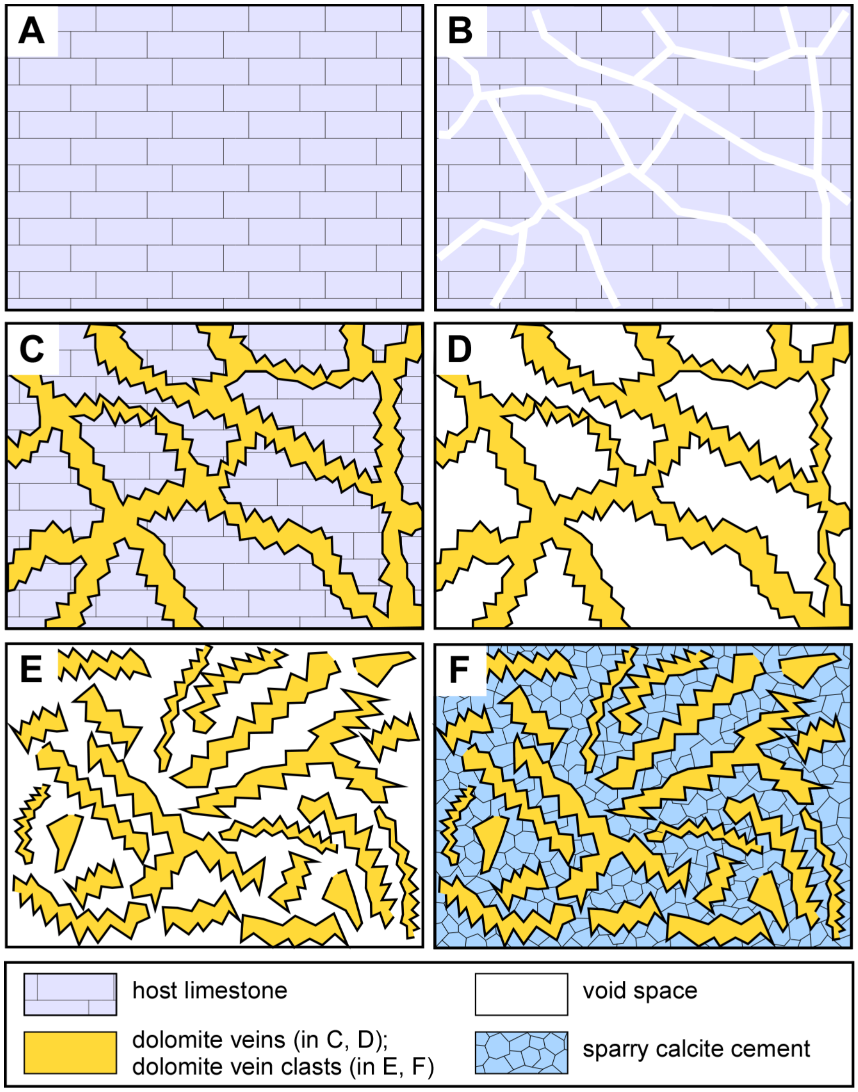

Fig. 20. (A–F) Interpretive sketch of the different steps leading to the formation of the type-4 breccias. A, B: the host limestone is crossed by a network of thin fractures. C: dolomitizing fluids flow through the fractures, resulting in dolomite cementation of the fractures and dolomitization of their walls. D: a local but complete dissolution of the host limestone occurs, leaving a frail network of isolated dolomite veins. E: the vein network collapses, forming clasts of vein material. F: clasts are cemented by sparry calcite.

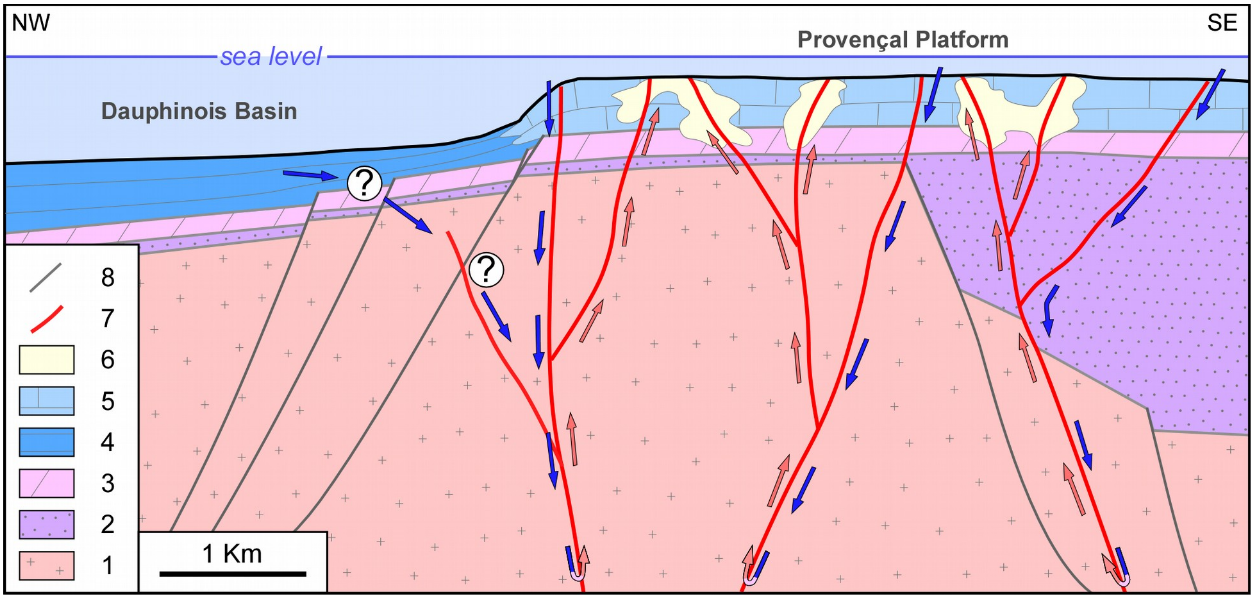

Fig. 21. Conceptual model illustrating the geometries of the hydrothermal system, and the hypothetical origin and circulation pathways of the fluids. Blue arrows represent cold descending fluids, whereas red arrows represent hot ascending fluids. Legend: 1: Argentera Massif crystalline basement. 2: Permian–Lower Triassic siliciclastic deposits. 3: Middle Triassic carbonates. 4: Jurassic Dauphinois hemipelagic succession. 5: Middle Jurassic–Berriasian Provençal carbonates (Garbella Limestone). 6: dolomitized bodies. 7: Early Cretaceous, syn-dolomitization faults. 8: inherited, Early Jurassic and Palaeozoic faults.

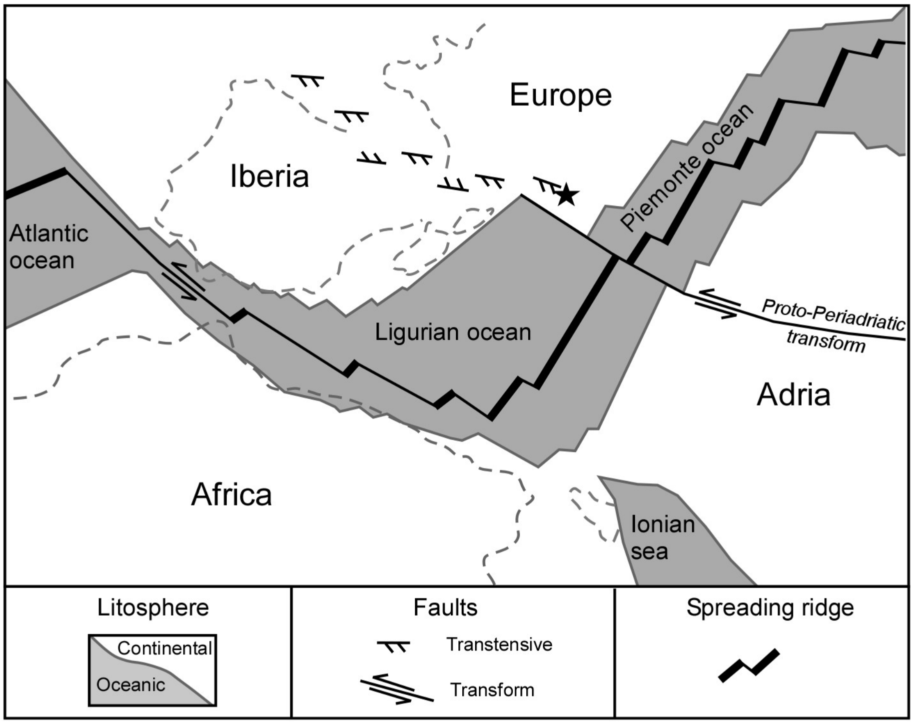

Fig. 22. Palaeogeographic sketch of the Western Mediterranean area in the Early Cretaceous. The black star indicates the position of the study area. Modified after Handy *et al*. (2010).